(4)

GL-TR-89-0192

SSS-TR-89-10755

NONLINEAR FINITE DIFFERENCE SIMULATIONS OF CAVITY DECOUPLED EXPLOSIONS IN SALT AND TUFF

J. L. Stevens
J. R. Murphy
N. Rimer

S-CUBED
Division of Maxwell Laboratories, Inc.
P. O. Box 1620
La Jolla, California 92038-1620

30 June 1989

Scientific Report No. 3

Geophysics Laboratory
Air Force Systems Command
United States Air Force
Hanscom Air Force Base
Massachusetts 01731-5000

SPONSORED BY
Defense Advanced Research Projects Agency
Nuclear Monitoring Research Office
ARPA ORDER NO. 5307

MONITORED BY
Geophysics Laboratory
Contract No. F19628-87-C-0093

This technical report has been reviewed and is approved for publication.

JAMES F. LEWKOWICZ
Contract Manager
Solid Earth Geophysics Branch
Earth Sciences Division

JAMES F. LEWKOWICZ
Branch Chief
Solid Earth Geophysics Branch
Earth Sciences Division

FOR THE COMMANDER

DONALD H. ECKHARDT, Director
Earth Sciences Division

This report has been reviewed by the ESD Public Affairs Office (PA) and is releasable to the National Technical Information Service (NTIS).

Qualified requestors may obtain additional copies from the Defense Technical Information Center. All others should apply to the National Technical Information Service.

If your address has changed, or if you wish to be removed from the mailing list, or if the addressee is no longer employed by your organization, please notify AFGL/DAA, Hanscom AFB, MA 01731-5000. This will assist us in maintaining a current mailing list.

Do not return copies of this report unless contractual obligations or notices on a specific document requires that it be returned.

UNCLASSIFIED
SECURITY CLASSIFICATION OF THIS PAGE

REPORT DOCUMENTATION PAGE

1a REPORT SECURITY CLASSIFICATION: UNCLASSIFIED	1b. RESTRICTIVE MARKINGS
2a SECURITY CLASSIFICATION AUTHORITY	3 DISTRIBUTION / AVAILABILITY OF REPORT: Approved for public release, distribution unlimited.
2b DECLASSIFICATION / DOWNGRADING SCHEDULE	
4 PERFORMING ORGANIZATION REPORT NUMBER(S): SSS-TR-89-10755	5. MONITORING ORGANIZATION REPORT NUMBER(S): GL-TR-89-0192
6a. NAME OF PERFORMING ORGANIZATION: S-CUBED, Division of Maxwell Laboratories, Inc. / 6b. OFFICE SYMBOL (If applicable)	7a. NAME OF MONITORING ORGANIZATION: Geophysics Laboratory
6c. ADDRESS (City, State, and ZIP Code): P. O. Box 1620, La Jolla, California 92038-1620	7b. ADDRESS (City, State, and ZIP Code): Hanscom Air Force Base, Massachusetts 01731-5000
8a. NAME OF FUNDING / SPONSORING ORGANIZATION: Defense Advanced Research Projects Agency / 8b OFFICE SYMBOL (If applicable): STO/GSD	9. PROCUREMENT INSTRUMENT IDENTIFICATION NUMBER: F19628-87-C-0093
8c. ADDRESS (City, State, and ZIP Code): 1400 Wilson Boulevard, Arlington, Virginia 22209	10. SOURCE OF FUNDING NUMBERS: PROGRAM ELEMENT NO 62714E; PROJECT NO 7A10; TASK NO DA; WORK UNIT ACCESSION NO DB

11. TITLE (Include Security Classification): NONLINEAR FINITE DIFFERENCE SIMULATIONS OF CAVITY DECOUPLED EXPLOSIONS IN SALT AND TUFF

12. PERSONAL AUTHOR(S): Stevens, J. L., Murphy, J. R. and Rimer, N.

13a. TYPE OF REPORT	13b. TIME COVERED	14. DATE OF REPORT (Year, Month, Day)	15. PAGE COUNT
Scientific No. 3	FROM 87/3/23 TO 89/3/22	89 June 30	68

16. SUPPLEMENTARY NOTATION

17 COSATI CODES			18. SUBJECT TERMS (Continue on reverse if necessary and identify by block number)
FIELD	GROUP	SUB-GROUP	Decoupling, Explosion, Seismology, Seismic Source, Nuclear Explosion, Overdecoupled Explosions, Tuff, Salt

19. ABSTRACT (Continue on reverse if necessary and identify by block number)

Nonlinear finite difference simulations are performed to model the seismic source functions for decoupled, partially coupled, and overdecoupled explosions in air-filled cavities in salt and unsaturated tuff emplacement media. The tuff simulations are performed in an 11 meter cavity under conditions similar to the Mill Yard experiment. The salt simulations are performed in a 17 meter cavity under conditions similar to the Sterling test.

The maximum low frequency decoupling factor in the tuff simulations is approximately 40. The low value of the decoupling factor is the result of the low shear modulus and poor tamped coupling of this material. The maximum decoupling factor is nearly twice a large as would be expected for a linear material model because the shock wave induces pore crushing that leads to a substantial loss of energy in the nonlinear case.

(Continued)

20. DISTRIBUTION / AVAILABILITY OF ABSTRACT	21 ABSTRACT SECURITY CLASSIFICATION	
☐ UNCLASSIFIED/UNLIMITED ☒ SAME AS RPT ☐ DTIC USERS	UNCLASSIFIED	
22a. NAME OF RESPONSIBLE INDIVIDUAL: James F. Lewkowicz	22b. TELEPHONE (Include Area Code)	22c. OFFICE SYMBOL: LWH

DD FORM 1473, 84 MAR — 83 APR edition may be used until exhausted. All other editions are obsolete. — SECURITY CLASSIFICATION OF THIS PAGE

18. Subject Terms (Continued)

Underdecoupled Explosions

19. Abstract (Continued)

The maximum low frequency decoupling factor in salt is approximately 100. In a 17 meter air-filled salt cavity, the explosion is fully decoupled at yields less than 0.2 kilotons, slightly less than the yield predicted using the Latter criterion. A low frequency decoupling factor of approximately 50 is predicted for a 1.5 kiloton explosion with the same material and geometry.

An important result of this research is that the low frequency source amplitude increases very slowly as the yield is increased above the yield required for full decoupling. In the materials studied, the decoupling factor decreases by only about a factor of two at a yield eight times the Latter decoupling criterion. These results suggest, for example, that it would be possible to detonate a 24 KT explosion in a cavity sufficient to fully decouple only a 3 KT explosion, and still achieve a decoupling ratio half as great as would be obtained from the much larger cavity that would be required to fully decouple the larger explosion.

At high frequencies, there is little difference between simulations with linear and nonlinear material models for decoupled or partially coupled explosions, except for attenuation due to pore crushing. All simulations show a strong high frequency peak due to cavity reverberations. The dominant frequency of this peak is a function of yield, increasing from about 100 Hz for the overdecoupled simulations to about 500 Hz for partially coupled simulations for the yields and cavity sizes studied here. Decoupling factors decrease as a function of frequency, however this decrease starts at higher frequencies for smaller, overdecoupled explosions than for larger, fully decoupled and partially coupled explosions. As a result, high frequency decoupling factors in the 30 to 50 Hz frequency band are larger for overdecoupled explosions than for fully decoupled explosions. Decoupling factors of less than one are predicted for frequencies higher than about 100 Hz for explosions in tuff.

TABLE OF CONTENTS

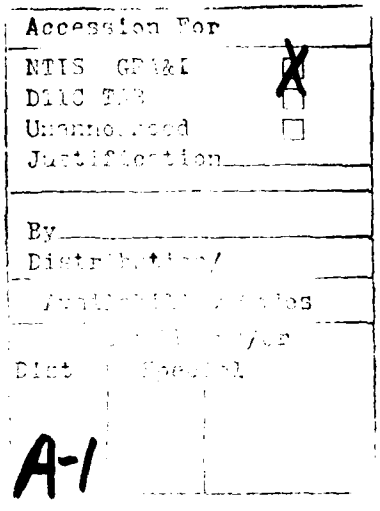

LIST OF ILLUSTRATIONS

LIST OF ILLUSTRATIONS (Continued)

LIST OF ILLUSTRATIONS (Concluded)

LIST OF TABLES

1. INTRODUCTION

It is well known that detonating an explosion in a cavity decouples the explosion source from the surrounding material, leading to sharply reduced seismic signals compared with a tamped explosion of the same yield. The possibility of such explosions being used as a means of avoiding detection has been a matter of serious concern for treaty verification. The theoretical decoupling factor is a strong function of frequency, and is largest at low frequencies. At high frequencies both the decoupling factor and the amplitude of the signal are reduced. This has led Evernden, *et al.* (1986) and others to suggest that it may be possible to detect and identify decoupled explosions using high frequency (> 20 Hz) seismic data.

The purpose of this study is to gain an improved understanding of the seismic source function of decoupled, partially coupled, and overdecoupled explosions at low and high frequencies, and to evaluate the implications of these predictions for detection and discrimination. In an earlier report (Murphy, *et al.*, 1988), we performed finite difference calculations in tuff and salt, and compared the results with data for the Mill Yard and Sterling experiments. The principal conclusions of that report based on this preliminary set of calculations were that:

1. A step pressure response is an inadequate model for a decoupled explosion. The air shock produces enhanced seismic coupling at high frequencies relative to a step pressure source.

2. The Latter decoupling criterion is approximately correct for salt, however nonlinearities due to pore crushing in tuff may occur at yields substantially less than the Latter criterion.

3. Because of pore crushing, decoupling effectiveness in tuff may be greater than decoupling effectiveness for an equivalent linear material. In salt, however, where the primary nonlinear effect is yielding, the nonlinear effects lead to increased coupling effectiveness.

4. Examination of free-field data from Sterling and Mill Yard indicates that high frequencies couple effectively into the seismic regime.

5. The observed complexity of high frequency propagation effects of the type observed at ground zero above the Mill Yard explosion makes it unlikely that differences in high frequency source characteristics can be reliably recovered from recorded seismic data.

In this report, we extend the earlier simulations to encompass a wider range of yields, and examine the seismic source functions for overdecoupled and underdecoupled explosions. In Sections 3 and 4 of this report, we present the results from a series of one dimensional finite difference simulations covering a range of yields in unsaturated tuff and salt cavities. Each set of calculations was repeated four times: first with a full nonlinear model of the cavity airshock and the emplacement material; second with a nonlinear model of the airshock, but with a linear material external to the cavity; third with a full nonlinear model of the material outside the cavity, but with the explosion applied as a step in pressure on the cavity wall; and fourth with a step pressure applied to a linear material. The linear material in each case has the same properties as the nonlinear material, except that it does not yield or undergo pore crushing. This set of calculations allows us to compare the full nonlinear results with results obtained from simpler calculations. In addition, we have performed finite difference simulations of tamped explosions using the full nonlinear models for salt and tuff. We compare these results with the decoupled simulations to determine the frequency dependent effects of decoupling.

2. REVIEW OF CAVITY DECOUPLED EXPLOSION THEORY

In this section, we review some fundamental theoretical relations for explosions in a cavity. These relations are used in the following sections of this report for comparison with the detailed results of finite difference calculations. The reduced velocity potential for a pressure pulse P(t), with derivative $\dot{P}(t)$, and corresponding Fourier transforms $P(\omega)$ and $\dot{P}(\omega)$ is given by:

$$\dot{\Psi}(\omega) = \dot{P}(\omega) \frac{R^3 \omega_0^2}{4\mu} \frac{e^{i\omega/\omega_0}}{\omega_0^2 - i\omega_0\omega - [(\lambda + 2\mu)/4\mu)]\omega^2} \qquad (2.1)$$

where $\omega_0 = \alpha/R$, R is the cavity radius, α is the compressional velocity of the external medium, and λ and μ are the Lame constants of the external medium. For a step in pressure of magnitude P_0 applied at time t = 0, $\dot{P}(\omega) = P_0$, and for this or any pressure pulse P(t) with static value P_0, in the low frequency limit $\dot{\Psi}(\omega)$ becomes:

$$\Psi_\infty = P_0 R^3/4\mu \qquad (2.2)$$

For an explosion in an air filled cavity, the static value of the pressure is related by conservation of energy to the explosion yield W by:

$$P_0 = \frac{(\gamma-1)\, W}{V} \qquad (2.3)$$

where $V = 4/3\pi R^3$ is the cavity volume, and γ is the adiabatic expansion constant which is approximately 1.2 for air. From Equations 2.2 and 2.3,

$$\Psi_\infty = \frac{3}{16\ \pi\mu} (\gamma-1)\, W \qquad (2.4)$$

Note that for a decoupled explosion, Ψ_∞ depends quite strongly on the shear modulus of the external medium. For the material models used in the following sections, the shear moduli are 3.5×10^9 Pascals, and 14.2×10^9 Pascals, for tuff and salt, respectively. Using a conversion factor of 4.1×10^{12} Joules/Kiloton for a nuclear explosion, we find for a decoupled explosion in tuff

$$\Psi_\infty \simeq 14.0 \text{ W} \tag{2.5}$$

and for a decoupled explosion in salt

$$\Psi_\infty \simeq 3.45 \text{ W} \tag{2.6}$$

where W is the yield in kilotons and Ψ_∞ is in m^3. Variations in γ also can cause significant variations in Ψ_∞.

The relative body wave amplitude A_b for explosion sources in dissimilar materials with the same propagation path is proportional to $\sqrt{\rho\alpha}\,\dot{\Psi}(\omega)$ (Stevens and Day, 1985), where ρ and α are the density and compressional velocity of the external medium, so from Equation 2.4 A_b is proportional to $\sqrt{\rho\alpha}/\mu$ W in the low frequency limit. Neglecting higher frequency spectral differences, therefore, A_b will be relatively larger for decoupled explosions in lower velocity media. This difference is approximately a factor of three for the salt and tuff models considered here.

The surface wave amplitude A_s of a decoupled explosion is proportional to $\mu\Psi(\omega)$, so A_s is independent of the material external to a decoupled explosion in the low frequency limit.

In the high frequency limit, Equation 2.1 reduces to

$$\dot{\Psi}\ \omega \sim -\dot{P}(\omega)\ \frac{\mathrm{Re}^{\,i\omega\cdot\omega_0}}{\rho\omega^2} \tag{2.7}$$

For a step function response, $\dot{P}(\omega)$ is equal to the static pressure P_0. As we discuss in the following two sections, however, $\dot{P}(\omega)$ may be quite complex at high frequencies because of cavity reverberations and the effect of the shock wave on the cavity wall. Also, certain nonlinear effects such as pore crushing cause the spectrum to decay more rapidly than ω^{-2} for partially coupled explosions.

In the high frequency limit, A_b becomes

$$A_b \sim \dot{P}(\omega) \sqrt{\alpha/\rho}\, R\, \omega^{-2} \tag{2.8}$$

so the dependence on material properties is in the factor $\sqrt{\alpha\rho}$. High frequency body waves are therefore less sensitive to material properties than lower frequency body waves. For the material models considered here, this factor is 30 percent larger for salt than for tuff.

Commonly used criteria for full decoupling are given by the relation

$$\frac{(\gamma-1)\,W}{\frac{4}{3}\pi R^3} \leq k\rho gh \tag{2.9}$$

where k is between 0.5 (Latter criterion, Latter, *et al.*, 1961), and 1.0 (Patterson criterion, Patterson, 1964), and ρgh is the overburden pressure at depth h.

In the following two sections, we consider explosions in an 11 meter radius tuff cavity with 62 bar overburden pressure, and a 17 meter salt cavity with 175 bar overburden pressure. For these two cases, the decoupling criteria range from 21 to 42 tons for tuff, and from 220 to 440 tons for salt.

3. FINITE DIFFERENCE SIMULATIONS OF EXPLOSIONS IN TUFF CAVITIES

We performed the set of cavity decoupled simulations described in the introduction over a range of yields from 5 to 160 tons for an 11 meter radius cavity in unsaturated tuff. The tuff model used here was described in our earlier report (Murphy, *et al.*, 1988), and is appropriate for Ranier Mesa tuff. This model has an initial porosity of 1.8 percent, and P and S wave speeds of 2558 m/sec and 1372 m/sec respectively.

A simulation of a tamped explosion in this material was run for comparison. In the low frequency limit, the tamped simulation leads to the result

$$\Psi_{tamped} \approx 325\ W \tag{3.1}$$

where W is the yield in kilotons and Ψ_{tamped} is in m^3. From Equation 2.5, therefore, the theoretical low frequency decoupling factor for this material, assuming γ of 1.2 and linear behavior of the medium, is given by:

$$D = \Psi_{tamped} / \Psi_{\infty} \approx 23 \tag{3.2}$$

As mentioned in the previous section, the decoupling factor is a material dependent quantity, and it depends quite strongly on both the shear modulus of the material and the tamped coupling of the material. For the tamped explosion, the final cavity radius is 14.3 $m/KT^{1/3}$, the radius of plastic yielding is 104 $m/KT^{1/3}$, and the pore crush radius is 157 $m/KT^{1/3}$. Note that in this material the transition to elastic behavior occurs at the limit of pore crushing rather than at the limit of plastic yielding.

In Tables 3.1 through 3.4, we summarize the results of these calculations. The columns in each table give the yield of the simulation, Ψ_{∞}, the peak value of the time domain reduced displacement potential Ψ_{peak}, the decoupling ratio D ($\Psi_{tamped}/\Psi_{\infty}$), the radius to limit of plastic yielding R_y, and the radius to the limit of pore crushing R_c.

TABLE 3.1

EXPLOSION IN 11 METER AIR-FILLED
TUFF CAVITY YIELD

Yield kt	ψ_∞ m^3	ψ_{peak} m^3	D	R_y m	R_c m
0.005	0.061	0.105	26.7	11.30	13.36
0.010	0.099	0.153	32.9	11.30	17.74
0.020	0.149	0.246	43.7	11.30	22.39
0.040	0.364	0.530	35.8	12.38	27.11
0.060	0.618	0.840	31.6	13.14	29.86
0.080	0.913	1.212	28.5	14.42	32.11
0.160	2.802	3.335	18.6	20.25	43.36

TABLE 3.2

EXPLOSION IN 11 METER AIR-FILLED
TUFF CAVITY: LINEAR

Yield kt	ψ_∞ m^3	ψ_{peak} m^3	D	R_y m	R_c m
0.005	0.069	0.110	23.6	11.00	11.00
0.010	0.139	0.195	23.4	11.00	11.00
0.020	0.293	0.371	22.2	11.00	11.00
0.040	0.579	0.692	22.5	11.00	11.00
0.060	0.841	0.976	23.2	11.00	11.00
0.080	1.084	1.266	24.0	11.00	11.00
0.160	2.187	2.504	23.8	11.00	11.00

TABLE 3.3

EXPLOSION IN 11 METER TUFF CAVITY - STEP PRESSURE

Yield kt	ψ_∞ m^3	ψ_{peak} m^3	D	R_y m	R_c m
0.005	0.092	0.106	17.7	11.00	11.00
0.010	0.156	0.177	20.9	11.00	11.00
0.020	0.279	0.317	23.3	11.00	11.00
0.040	0.477	0.540	27.3	11.00	11.00
0.060	0.689	0.781	28.3	11.00	11.00
0.080	0.940	1.067	27.7	11.00	11.00
0.160	2.009	2.275	25.9	11.00	11.00

TABLE 3.4

EXPLOSION IN 11 METER TUFF CAVITY -
STEP PRESSURE: LINEAR

Yield kt	ψ_∞ m^3	ψ_{peak} m^3	D	R_y m	R_c m
0.005	0.093	0.104	17.5	11.30	11.00
0.010	0.155	0.175	21.0	11.30	11.00
0.020	0.278	0.315	23.4	11.30	11.00
0.040	0.475	0.539	27.4	11.30	11.00
0.060	0.687	0.778	28.4	11.30	12.32
0.080	0.930	1.053	28.0	11.30	16.57
0.160	2.408	2.641	21.6	16.93	29.87

In Figure 3.1, we show the low frequency decoupling factor for the air-filled linear and nonlinear cases listed in Tables 3.1 and 3.2. The Latter criterion for full decoupling in this material is 21 tons. As can be seen from the tables, the nonlinear material behavior is too complex to be described by a single number. For a model with a true air shock inside the cavity, yielding begins with an explosion yield of between 20 and 40 tons, however pore crushup begins with explosion yields as small as 5 tons. The effect of pore crushup is to remove energy from the outgoing seismic wave, so it has the effect of increasing decoupling. As a result, the maximum low frequency decoupling factor of 44 is achieved with a yield of 20 tons, which exceeds the decoupling factor of 23 predicted with a linear material model. With higher explosion yields, the decoupling effectiveness decreases as yielding becomes the dominant effect. At 160 tons, the decoupling factor decreases to less than that for a linear model. For the linear models, the low frequency decoupling ratio is close to the value of 23 predicted from simple theory. The differences from this value result from the differences in the equation of state for air at different energy levels.

In Figures 3.2 through 3.6, we show the reduced velocity potentials for all seven yields for each set of calculations. Care was taken in the calculations to preserve the high frequencies by using fine zoning and a low value for artificial viscosity. The results are accurate to approximately 500 hz. Above this frequency, the spectral amplitudes are gradually reduced by artificial viscosity. All of the cavity calculations containing an airshock show a high frequency peak corresponding to cavity reverberations. For the smallest yield of 5 tons, the air shock reverberations dominate the spectrum. The dominant frequency of this peak increases with yield, ranging from 100 Hz for the 5 ton calculation to 600 hz for the 160 ton calculation. This result indicates that the high frequency enhancement due to cavity reverberations is more likely to be observed from an overdecoupled explosion than from a fully decoupled or partially decoupled explosion. Note that these frequencies will cube root scale to other yields and geometries provided that the ratio of the yield to cavity volume is kept constant.

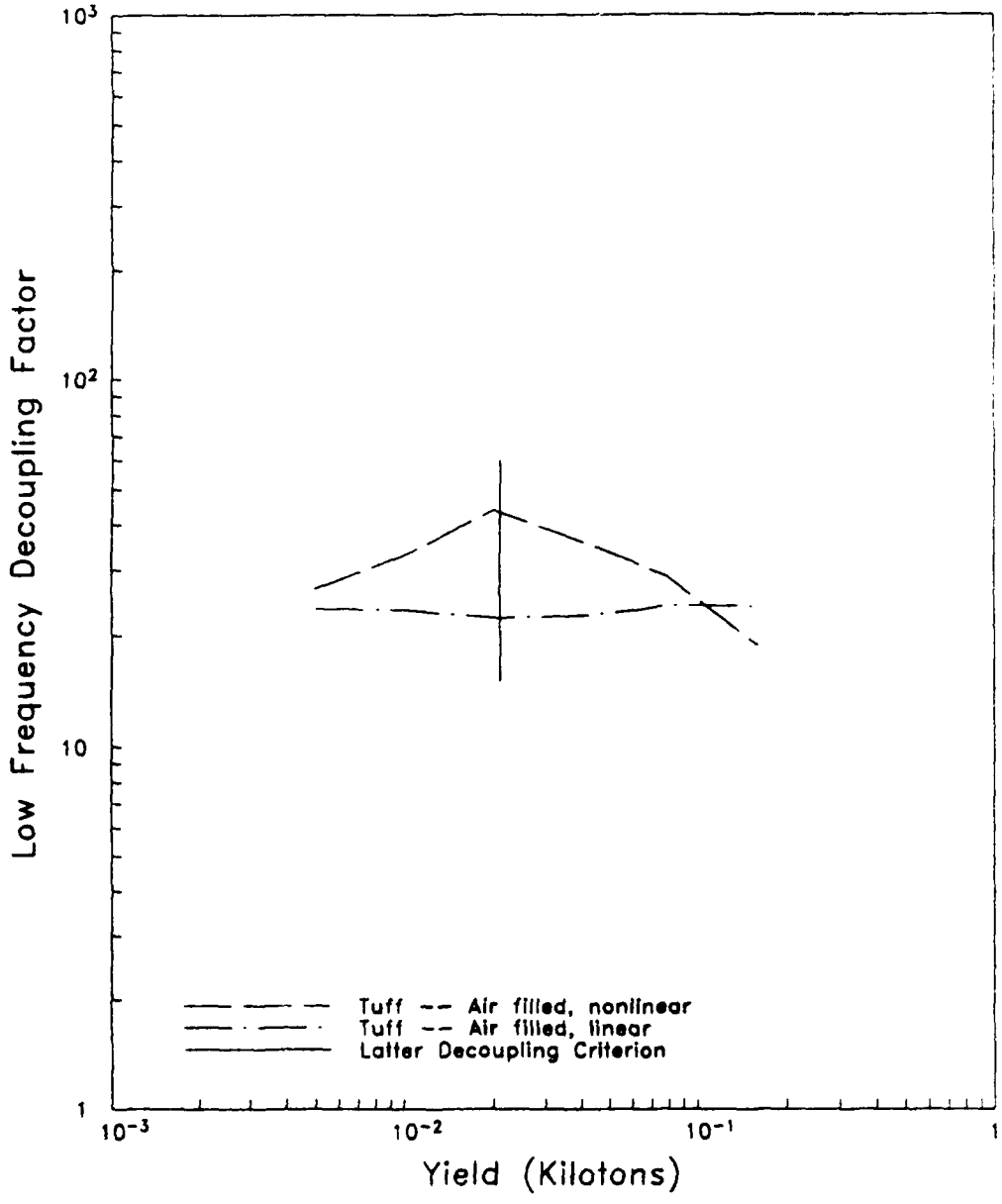

Figure 3.1. Low frequency decoupling factor plotted as a function of yield for the air-filled linear and nonlinear tuff simulations. The decoupling factor is defined to be the ratio of the tamped reduced velocity potential to the decoupled reduced velocity potential with the same material properties used for both calculations. The vertical line indicates the yield corresponding to the Latter decoupling criterion for this material and geometry. The peak in the nonlinear decoupling factor is due to the effect of pore crushing which reduces the low frequency source function.

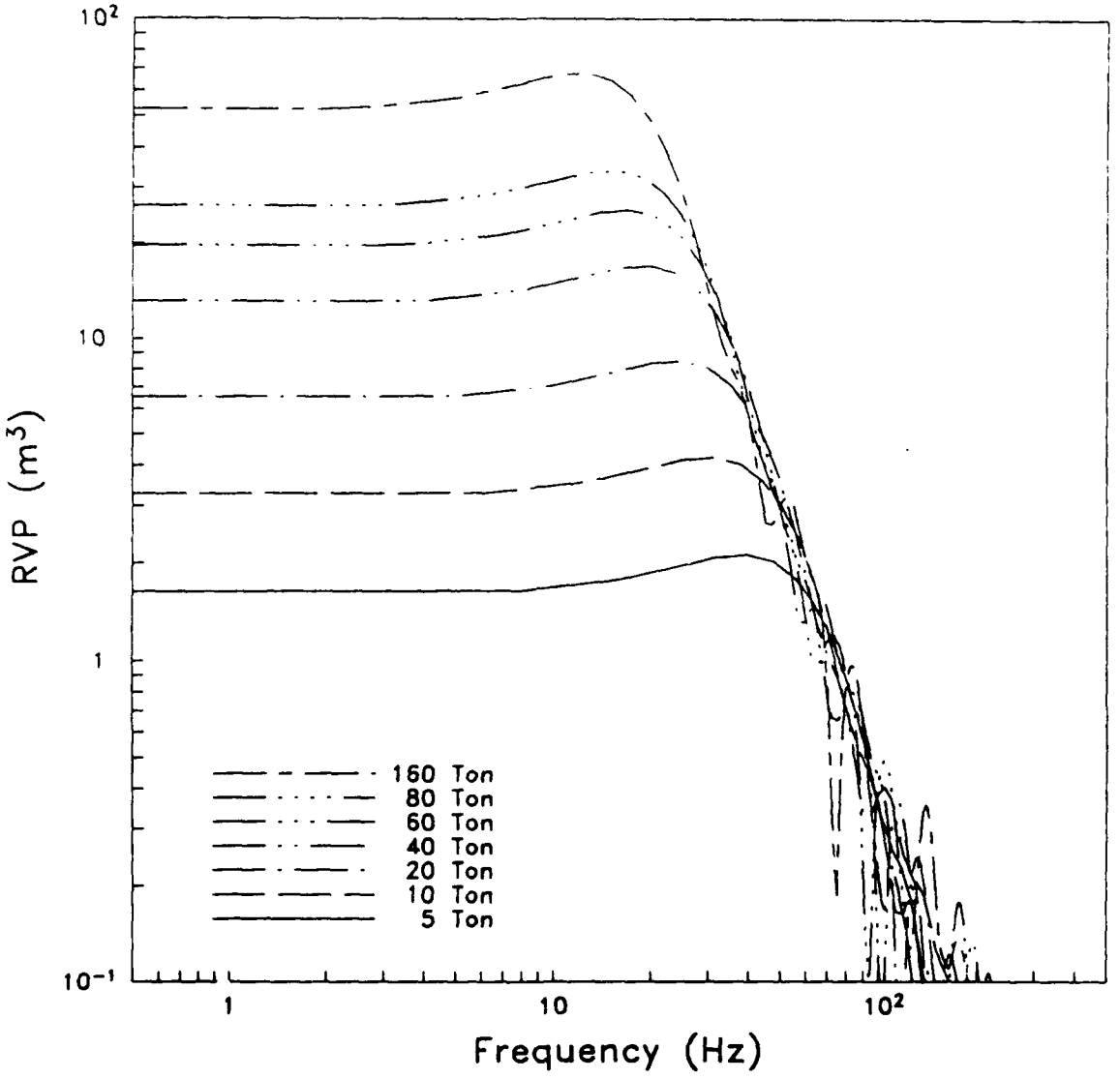

Figure 3.2. Reduced velocity potential for a tamped explosion in unsaturated tuff, scaled to seven different yields.

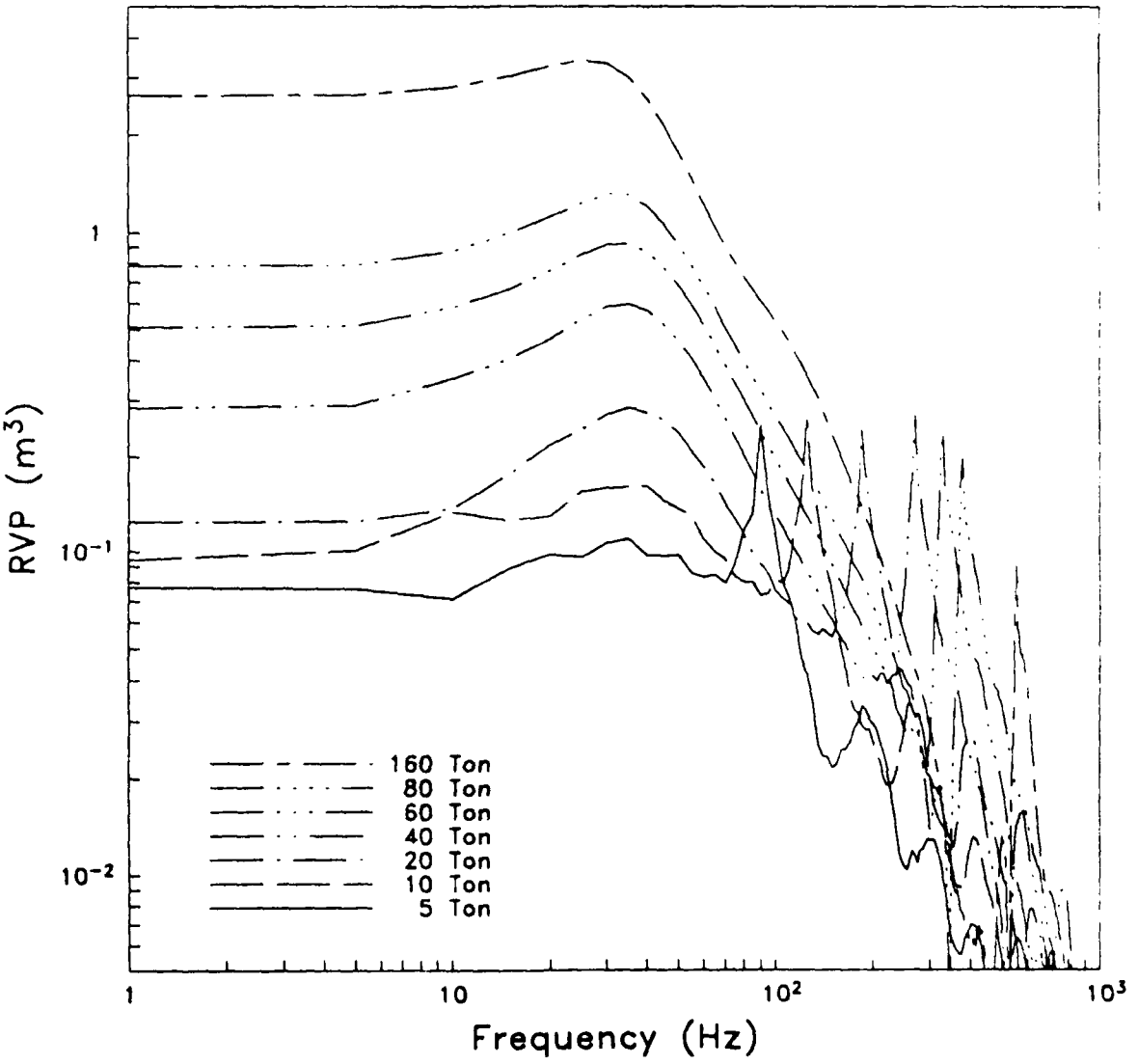

Figure 3.3. Reduced velocity potential for seven different yields for an air filled cavity inside a medium with a nonlinear tuff material model.

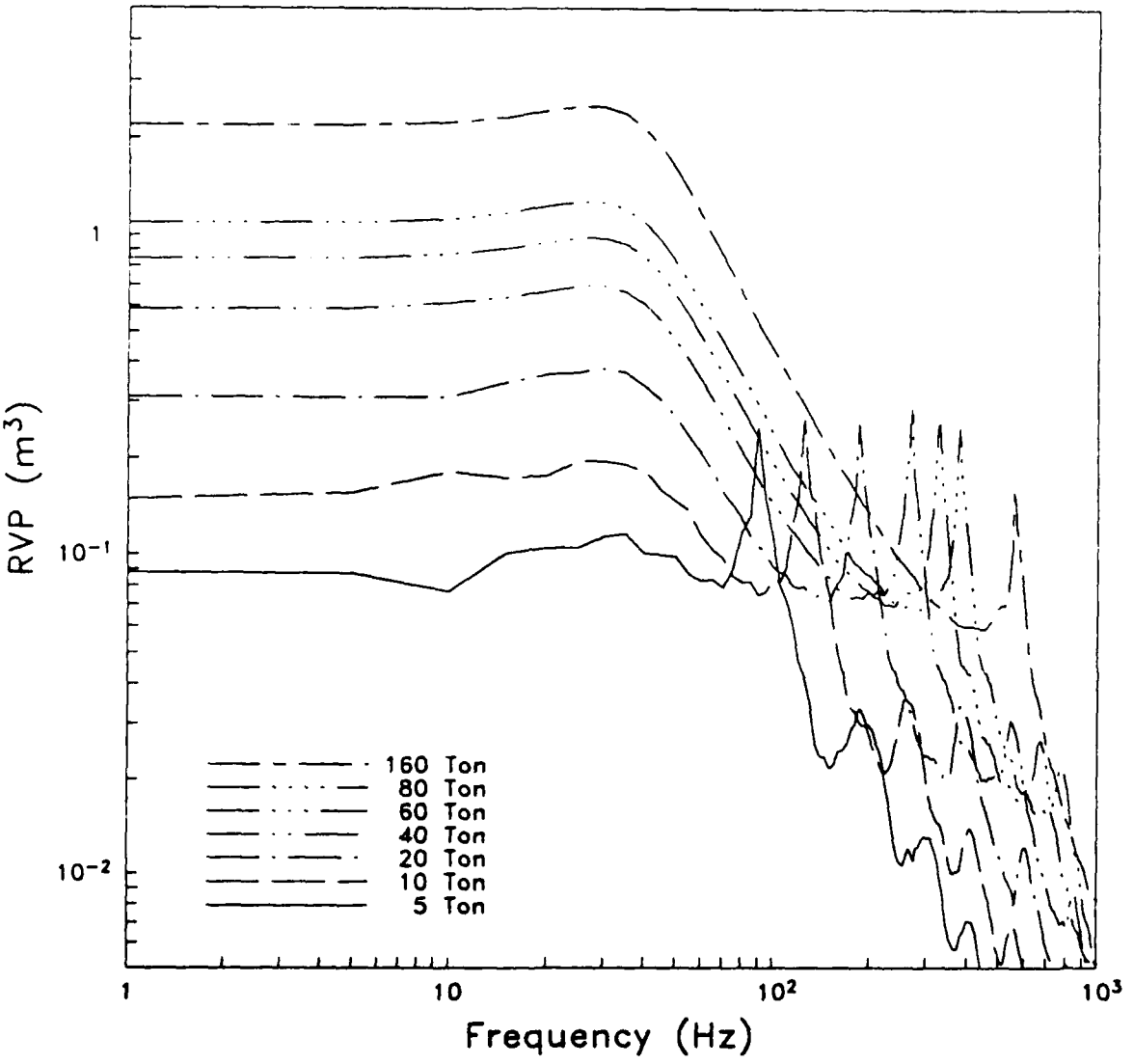

Figure 3.4. Reduced velocity potential for seven different yields for an air filled cavity inside a medium with a linear tuff material model.

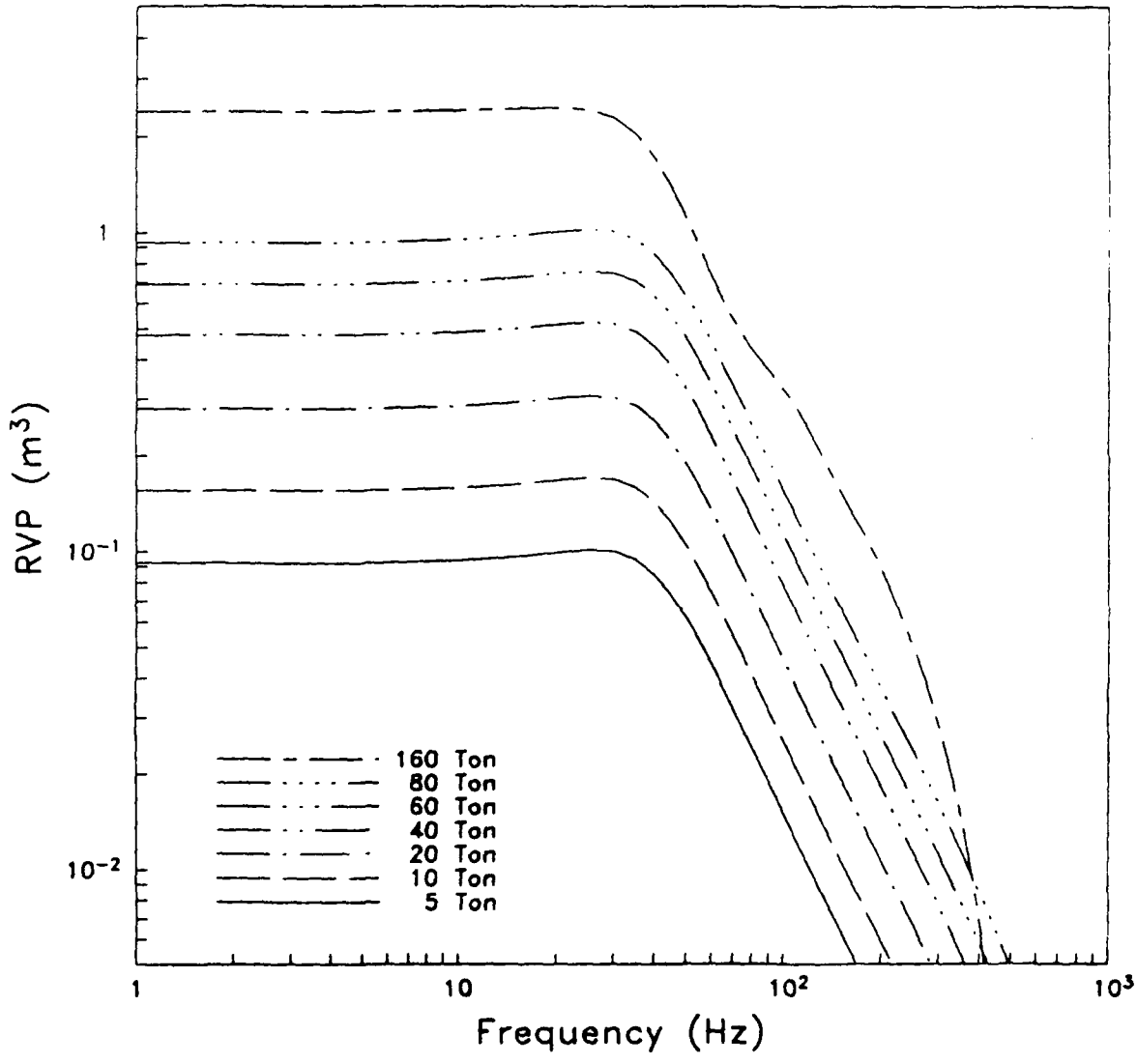

Figure 3.5. Reduced velocity potential for seven different yields for a step pressure on a cavity inside a medium with a nonlinear tuff material model.

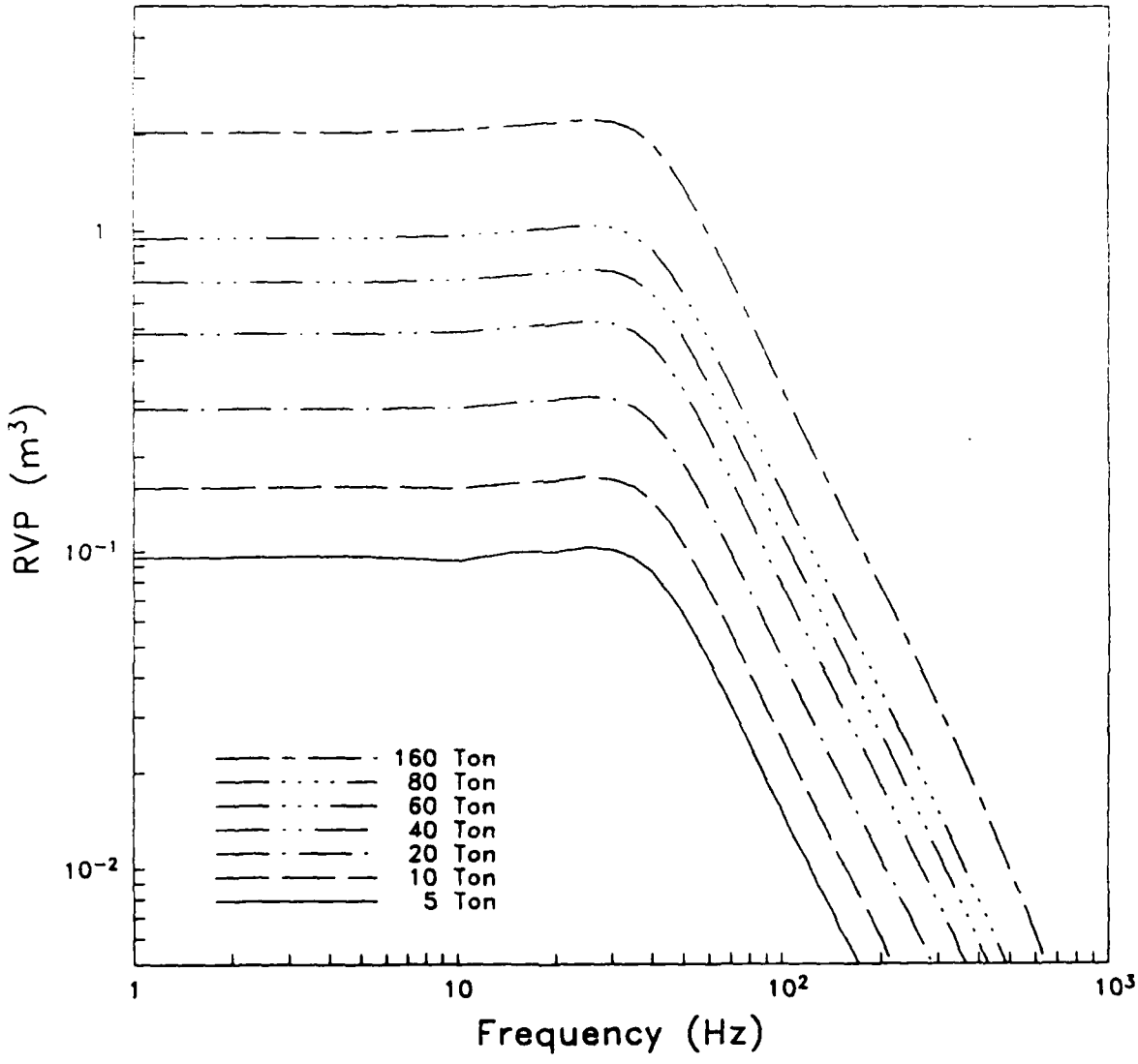

Figure 3.6. Reduced velocity potential for seven different yields for a step pressure on a cavity inside a medium with a linear tuff material model.

In Figures 3.7 through 3.10, we show the decoupling factors for each of the simulations, plotted as a function of frequency. These decoupling factors were determined by cube-root scaling the tamped explosion spectrum to the same yield as the cavity simulation, and then taking the ratio of tamped to cavity spectra. At low frequencies, there are significant differences between the linear and nonlinear simulations. At high frequencies, however, the cavity reverberations dominate the spectrum. The only significant difference between the linear and nonlinear calculations at high frequency is that the nonlinear spectra are attenuated by pore crushing. Because the cavity reverberations generate a substantial amount of high frequency energy, the high frequency decoupling factors are significantly lower for the air-filled cavity simulations than for the step pressure calculations. Because the nonlinear effects cause attenuation of high frequencies in the tamped case, however, the decoupling factors drop off rapidly at high frequency, and are reduced to less than one at sufficiently high frequency in all cases.

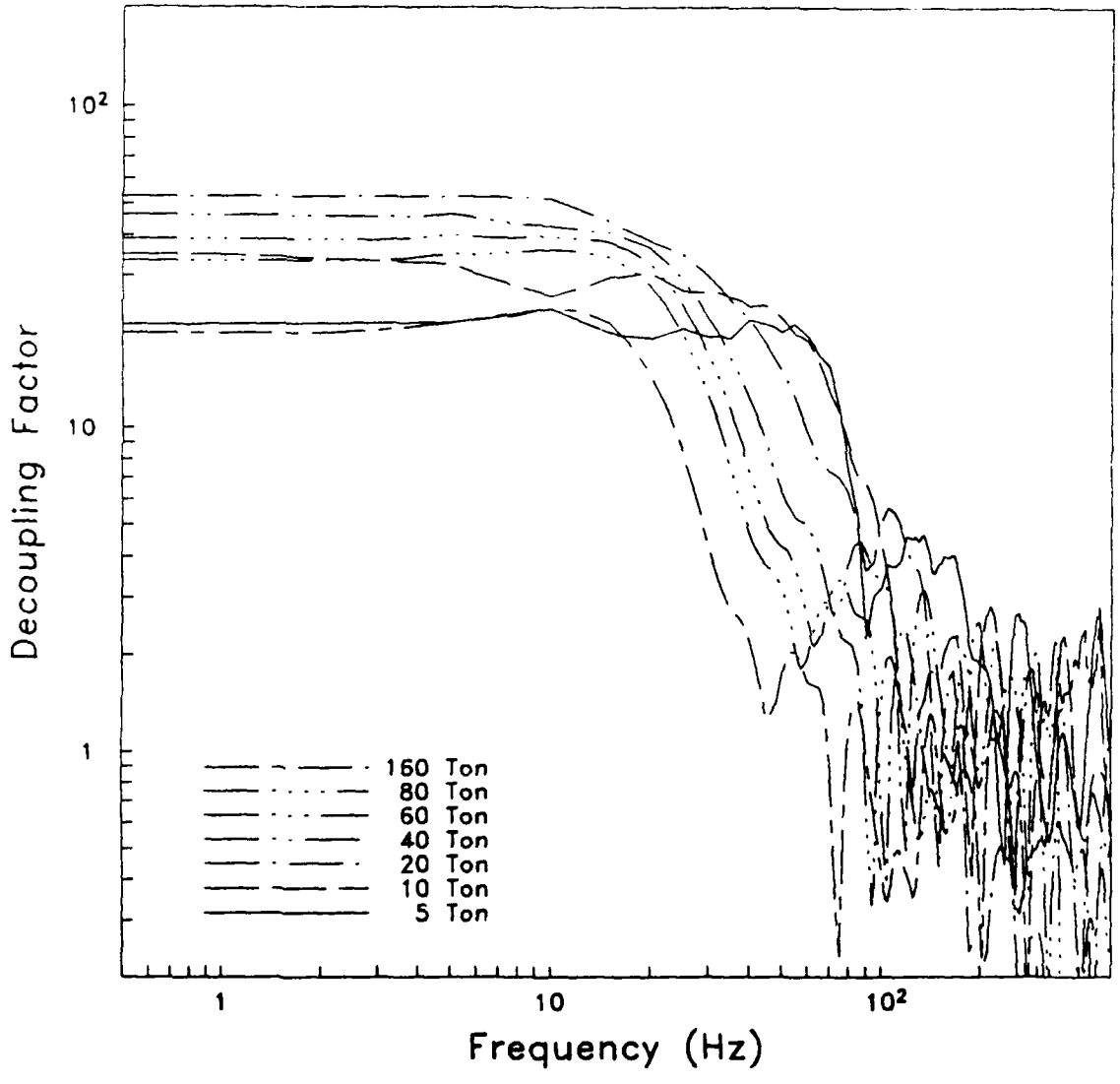

Figure 3.7. Frequency dependent decoupling factor for seven different yields for an air filled cavity inside a medium with a nonlinear tuff material model.

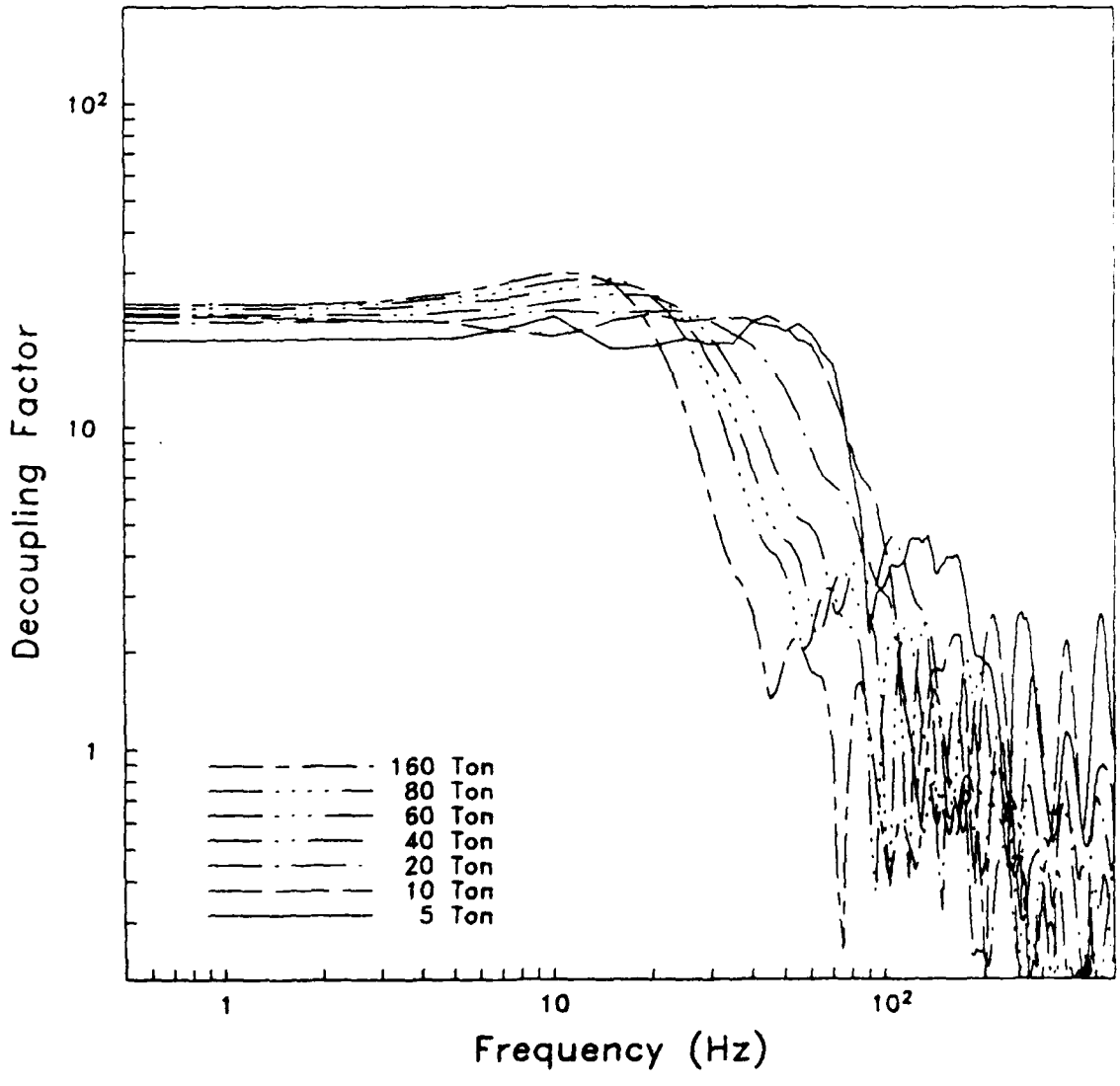

Figure 3.8. Frequency dependent decoupling factor for seven different yields for an air filled cavity inside a medium with a linear tuff material model.

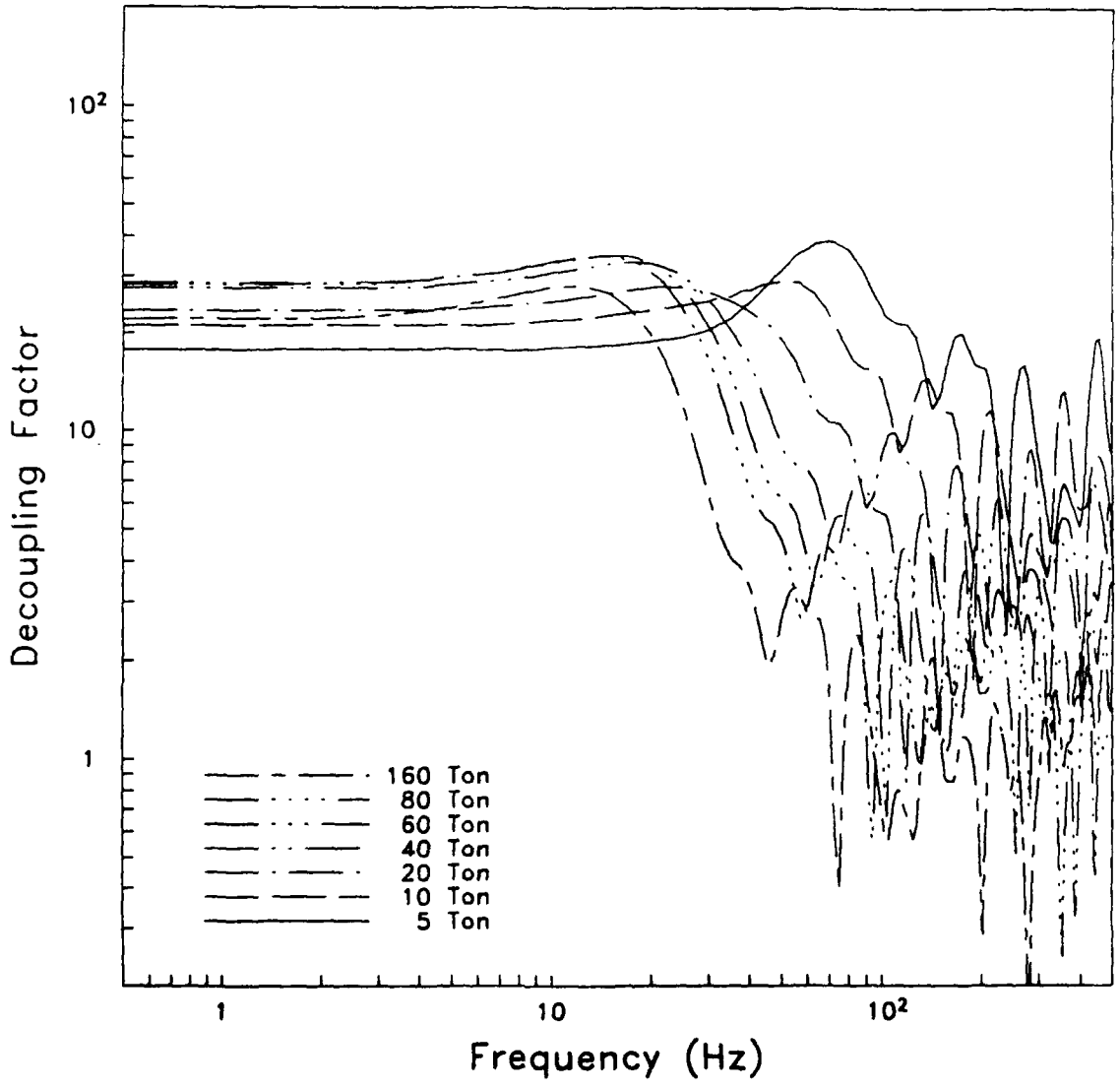

Figure 3.9. Frequency dependent decoupling factor for seven different yields for a step pressure on a cavity inside a medium with a nonlinear tuff material model.

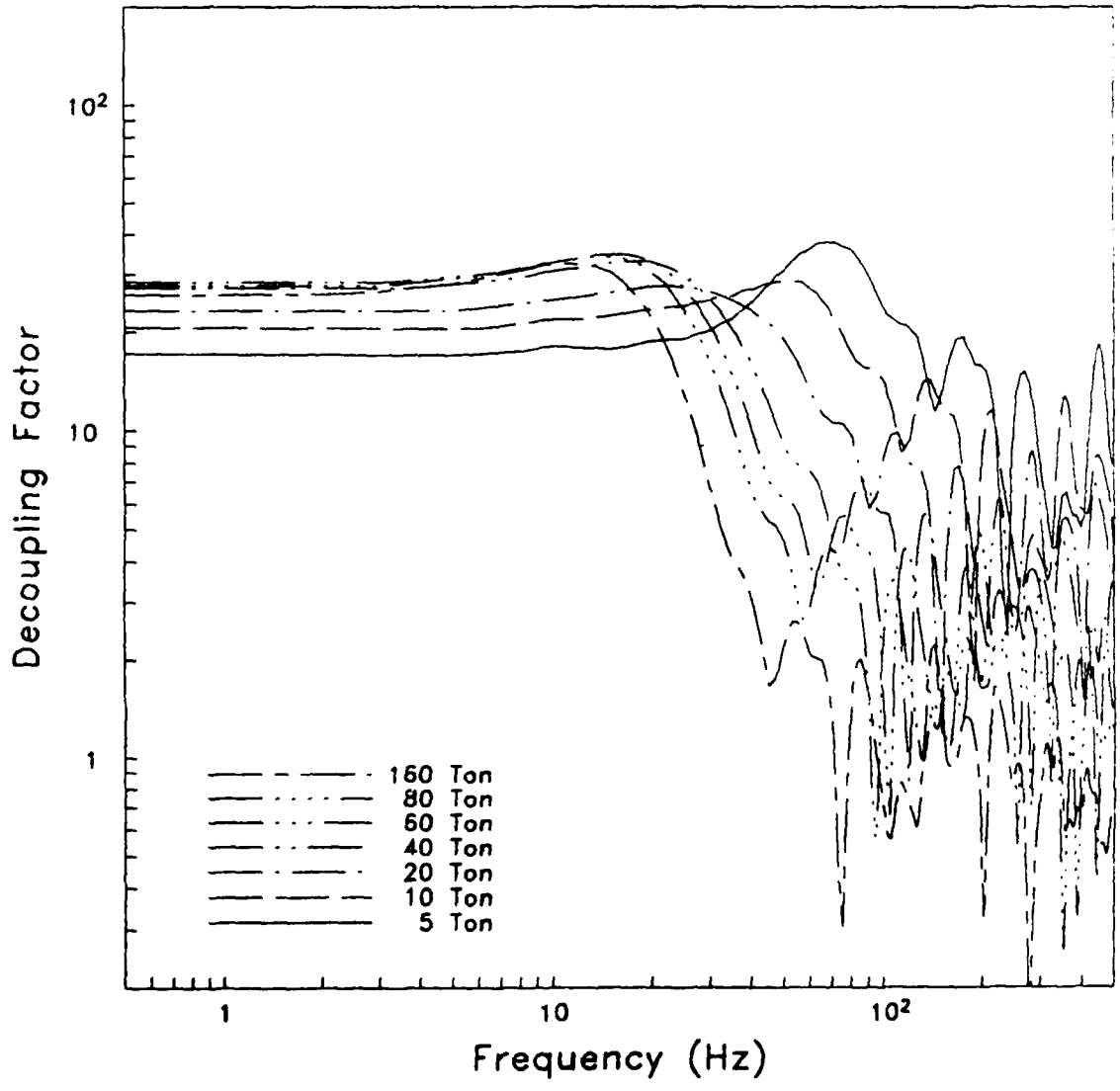

Figure 3.10. Frequency dependent decoupling factor for seven different yields for a step pressure on a cavity inside a medium with a linear tuff material model.

4. FINITE DIFFERENCE SIMULATIONS OF EXPLOSIONS IN SALT CAVITIES

We performed the set of cavity decoupled simulations described in the introduction over a range of yields from 95 to 1520 tons for a 17 meter radius cavity in salt. The constitutive model used in these calculations was based on the results of laboratory material property tests on polycrystalline salt (Heard, *et al.*, 1975). We also made some test calculations using the earlier hardening/softening model of Rimer and Cherry (1982). This earlier model produced an excellent comparison with the nearfield Salmon data, however it was found to be too weak to maintain a 17 meter cavity at this depth without undergoing very substantial nonlinear deformation. A test calculation using a 17 meter cavity in this material showed that it stabilizes after undergoing a surface displacement (inward) of 2 centimeters, and plastic deformation extending to 70 meters. Since the Sterling cavity was generated by the Salmon explosion, however, it is not clear what initial conditions to use for studying partially coupled explosions in this material. A cavity constructed in this material would develop a hardened core extending to a considerable distance away from the cavity. The calculations in this section have been performed using the polycrystalline salt model described above which is strong enough to support a stable cavity. Some calculations have also been performed using the much weaker Rimer/Cherry model for the air-filled, partially coupled cases, and the results are shown for comparison in some of the figures in this section.

In Figure 4.1, we show a comparison of particle velocities at four locations from the simulation at 0.38 KT, with the observed particle velocities from the Sterling explosion. The data cannot be fit exactly with a spherically symmetric model, since measured particle velocities at the same radial distance at angles obliquely above and below the explosion differ in amplitude by about a factor of two. Nevertheless, the model appears to provide a reasonably good representation of the Sterling data.

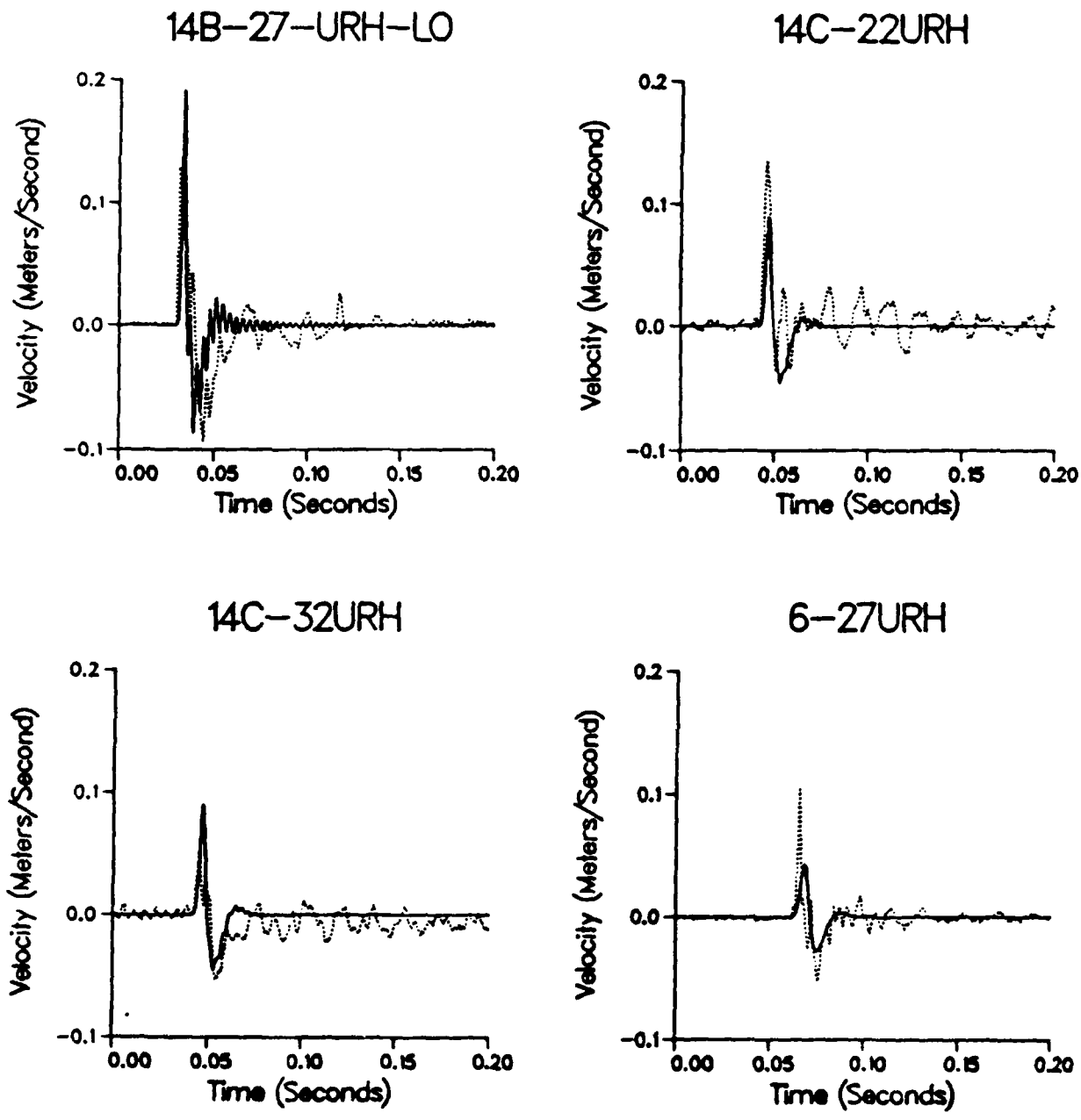

Figure 4.1. Comparison of data from the Sterling explosion with calculation of a 0.38 KT explosion in an air filled 17 meter cavity using the nonlinear material model described in the text. The data points were advanced by 6 msec. 14B-27 is at shot depth, 166 meters from the explosion. 14C-22 is above shot depth, 225 meters from the explosion. 14C-32 is below shot depth, 225 meters from the explosion. 6-27 is at shot depth, 318 meters from the explosion.

A simulation of a tamped explosion in this material was run for comparison. In the low frequency limit, the tamped simulation gives the result

$$\Psi_{tamped} = 320\ W \tag{4.1}$$

where W is the yield in kilotons. From Equation 2.6, therefore, the theoretical low frequency decoupling factor for this material is given by:

$$D = \Psi_{tamped}/\Psi_{\infty} \simeq 93 \tag{4.2}$$

In Tables 4.1 through 4.4, we summarize the results of these calculations. The columns in each table give the yield of the simulation, Ψ_{∞}, the peak value of the time domain reduced displacement potential Ψ_{peak}, the decoupling ratio D ($\Psi_{tamped}/\Psi_{\infty}$), and the radius to limit of plastic yielding R_y. There is no pore crush radius in this case, because the salt is assumed to be nonporous. For this tamped explosion, the cavity radius is 12.0 m/KT$^{1/3}$, and the elastic radius is 112 m/KT$^{1/3}$.

In Figure 4.2, we show the low frequency decoupling ratio plotted as a function of yield for the air-filled linear and nonlinear cases. We also show results calculated using the Rimer/Cherry model for comparison. The Latter criterion for full decoupling in this material is 220 tons. As can be seen from the tables and Figure 4.2, yielding begins at slightly less than 190 tons for the full nonlinear case. With the step function source model, there is no plastic yielding for explosion yields less than about a kiloton for this material. The decoupling factor, however, remains about the same over a large range of explosion yields, and decreases by only a factor of 2 at 1520 tons, even though the elastic radius has increased to 33 meters. This slow decrease in decoupling is also true for the Rimer/Cherry model. Even though this model is initially very weak, and is not linear at any yield used in this set of simulations, the decoupling factor has decreased by only about a factor of four at 1520 tons yield. It can be seen from this figure that the main features of the decoupling calculations are not particularly sensitive to the material model employed in that all of the calculations indicate that the low frequency decoupling effectiveness decreases quite slowly with increasing yield above the Latter threshold.

TABLE 4.1

EXPLOSION IN 17 METER AIR-FILLED SALT CAVITY

Yield kt	Ψ_∞ m^3	Ψ_{peak} m^3	D	R_y m
0.095	0.297	0.413	101.7	17.00
0.138	0.453	0.613	96.9	17.00
0.190	0.732	0.904	82.6	17.94
0.276	1.151	1.397	76.3	18.53
0.380	1.683	2.003	71.8	19.49
0.570	2.909	3.339	62.3	20.82
0.760	4.135	4.723	58.5	22.01
1.520	10.375	11.545	46.6	33.27

TABLE 4.2

EXPLOSION IN 17 METER AIR-FILLED SALT CAVITY: LINEAR

Yield kt	Ψ_∞ m^3	Ψ_{peak} m^3	D	R_y m
0.095	0.297	0.413	101.7	17.00
0.138	0.453	0.613	96.9	17.00
0.190	0.721	0.860	83.8	17.00
0.276	0.996	1.207	88.1	17.00
0.380	1.309	1.560	92.3	17.00
0.570	1.962	2.259	92.4	17.00
0.760	2.597	2.989	93.1	17.00
1.520	5.669	6.367	85.3	17.00

TABLE 4.3

EXPLOSION IN 17 METER SALT CAVITY - STEP PRESSURE

Yield kt	ψ_∞ m^3	ψ_{peak} m^3	D	R_y m
0.095	0.294	0.340	102.8	17.00
0.138	0.413	0.457	106.3	17.00
0.190	0.542	0.606	111.5	17.00
0.276	0.774	0.889	113.4	17.00
0.380	1.149	1.280	105.2	17.00
0.570	1.753	1.970	103.4	17.00
0.760	2.332	2.615	103.7	17.00
1.520	6.321	6.859	76.5	24.61

TABLE 4.4

EXPLOSION IN 17 METER SALT CAVITY -
STEP PRESSURE: LINEAR

Yield kt	ψ_∞ m^3	ψ_{peak} m^3	D	R_y m
0.095	0.294	0.340	102.8	17.00
0.138	0.413	0.457	106.3	17.00
0.190	0.542	0.606	111.5	17.00
0.276	0.774	0.889	113.4	17.00
0.380	1.149	1.280	105.2	17.00
0.570	1.753	1.970	103.4	17.00
0.760	2.332	2.615	103.7	17.00
1.520	5.241	5.872	92.2	17.00

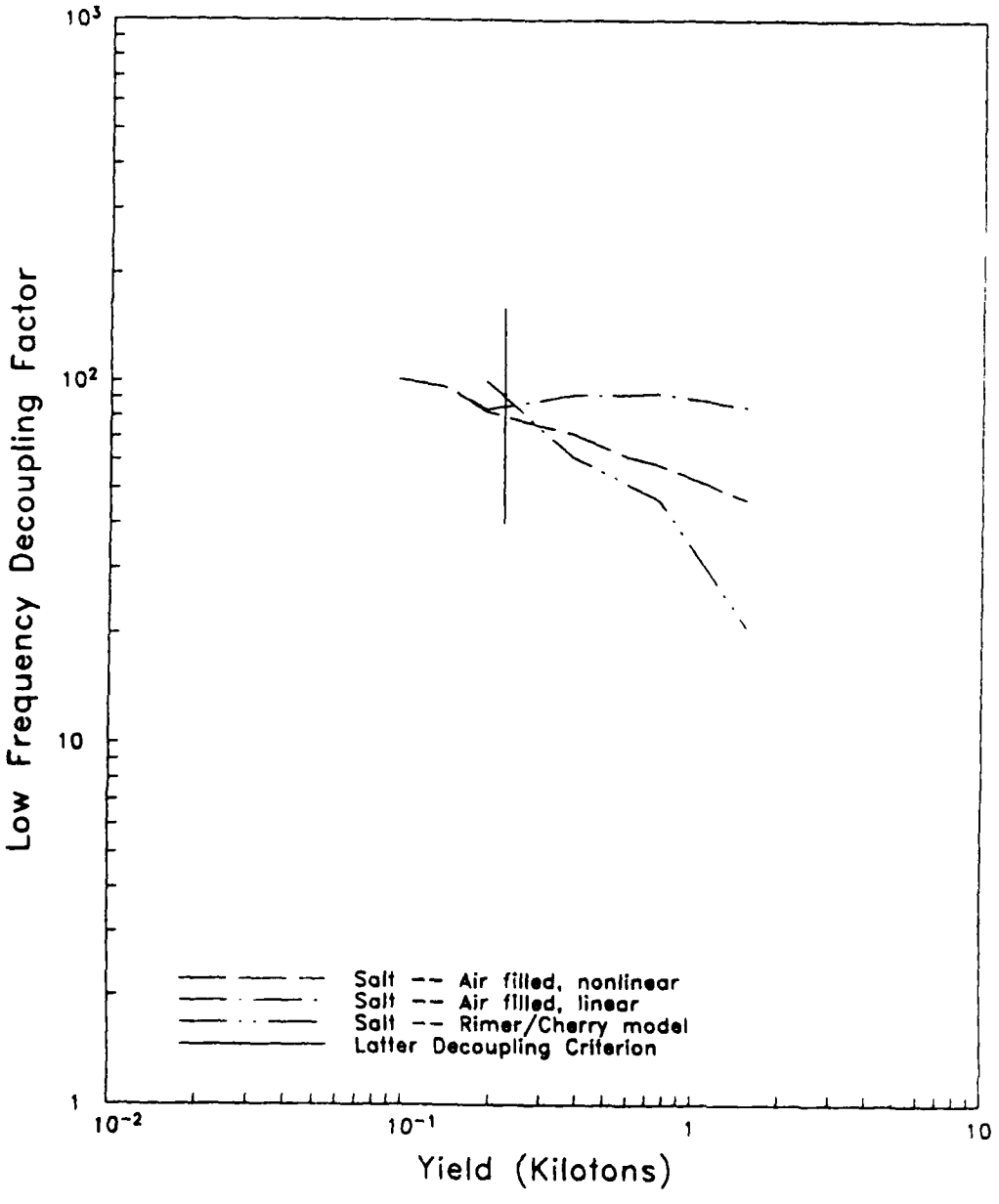

Figure 4.2. Low frequency decoupling factor plotted as a function of yield for the air-filled linear and nonlinear salt simulations. Also shown are decoupling factors calculated using the weaker Rimer/Cherry salt model. The vertical line indicates the yield corresponding to the Latter decoupling criterion for this material and geometry. The decoupling factors decrease by only a factor of between two and four at the highest yield calculated.

In Figure 4.3 we show a comparison of the normalized low frequency decoupling factors obtained from our calculations and those of Patterson (1964) with the observed decoupling values from the COWBOY HE decoupling tests which covered the widest available range of ratios of yield to cavity volume. In order to compare the dependence of decoupling effectiveness on cavity size, the three theoretical curves in Figure 4.3 have been normalized to the observed COWBOY full decoupling value of 70. It can be seen that all three sets of calculations are in qualitative agreement with the limited data and indicate that the decoupling effectiveness decreases fairly slowly with increasing yield over the range investigated in this report. However, in detail, the somewhat more rapid decrease predicted using the weak Rimer/Cherry salt model does seem to provide somewhat better agreement with the two COWBOY HE data points associated with the largest overdrive values.

In Figures 4.4 through 4.8, we show the reduced velocity potentials for all eight yields for each set of calculations. As with the tuff models, all of the calculations containing an airshock show a high frequency peak corresponding to cavity reverberations. Again, the frequency of the peak increases with yield, ranging from just over 100 Hz for the 95 ton simulation, to about 600 Hz for the 1520 ton simulation. In all cases, there is little difference between the linear and nonlinear simulations at high frequencies.

In Figures 4.9 through 4.12, we show the decoupling ratio for each of the simulations. The results are very similar to the tuff simulations. The air-filled cavity simulations have lower decoupling ratios than the step pressure simulations at high frequencies, particularly for overdecoupled explosions. Decoupling ratios drop off at high frequencies, however the dropoff occurs at higher frequencies for lower yield explosions than for higher yield explosions.

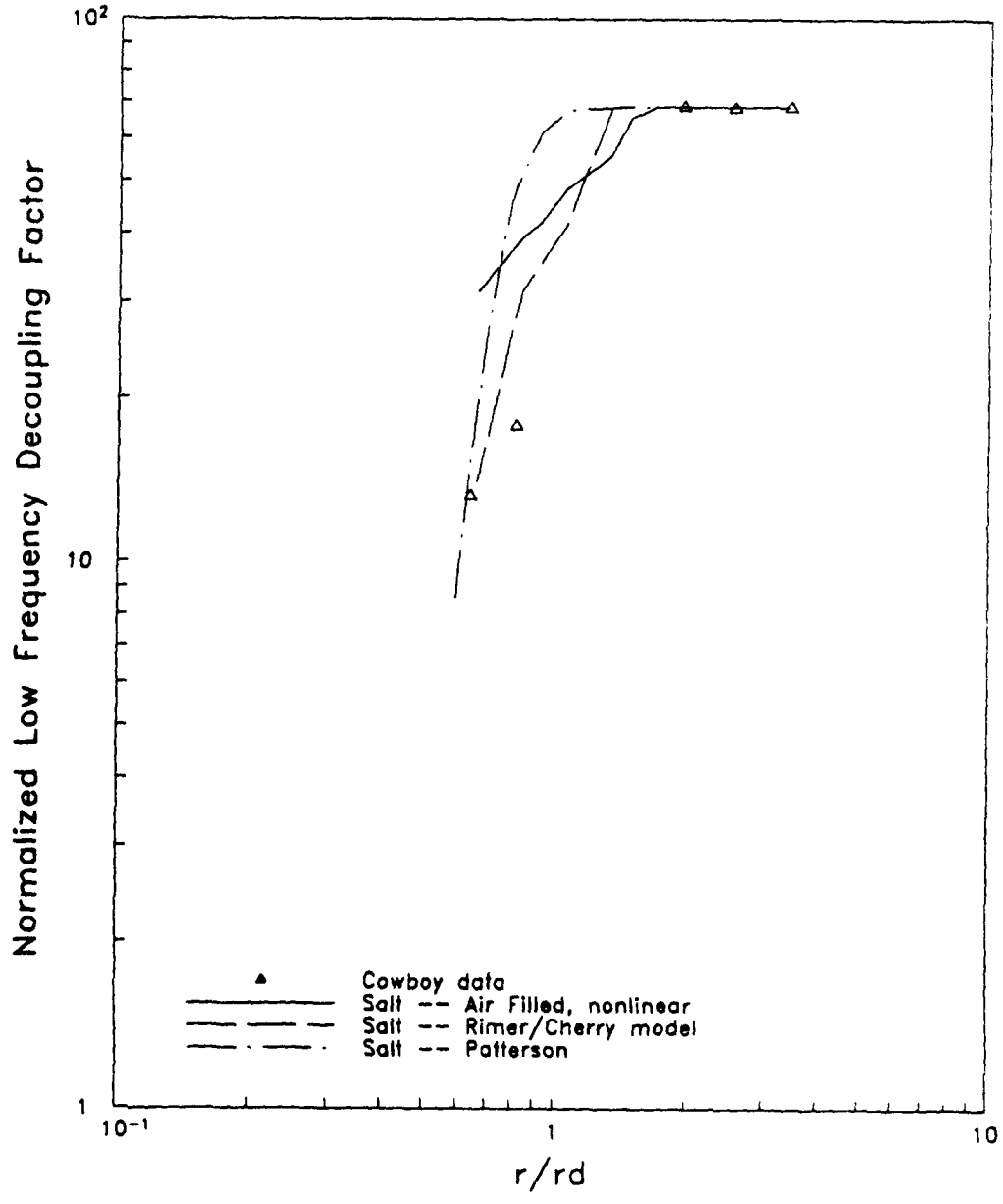

Figure 4.3. Low frequency decoupling factors for the air-filled nonlinear salt model, together with decoupling factors calculated with the Rimer/Cherry model, the finite difference calculations of Patterson (1964), and data points from the Cowboy experiment. These are plotted against the dimensionless quantity r/r_d where r_d is the radius for "full" decoupling.

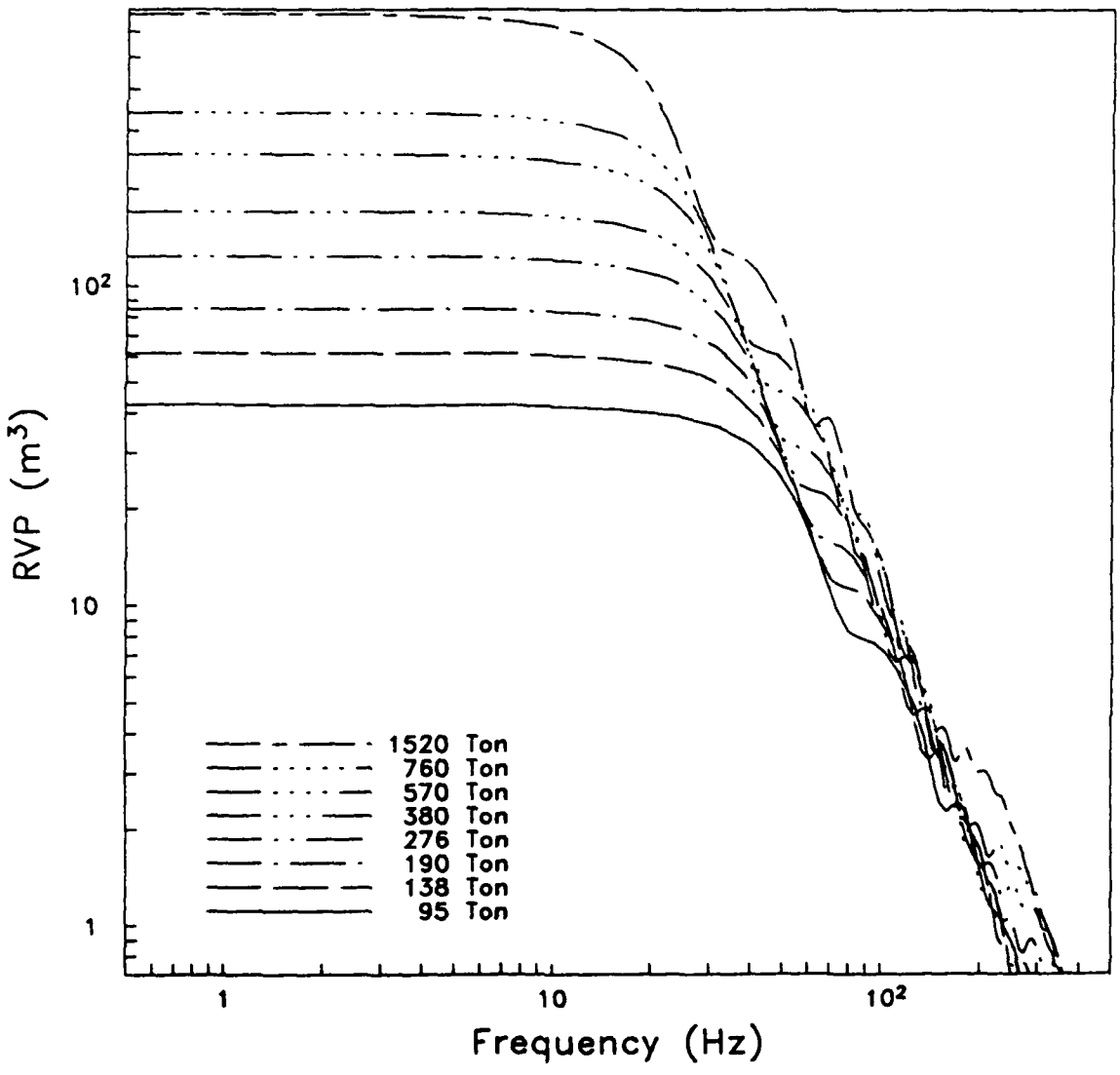

Figure 4.4. Reduced velocity potential for a tamped explosion in salt, scaled to eight different yields.

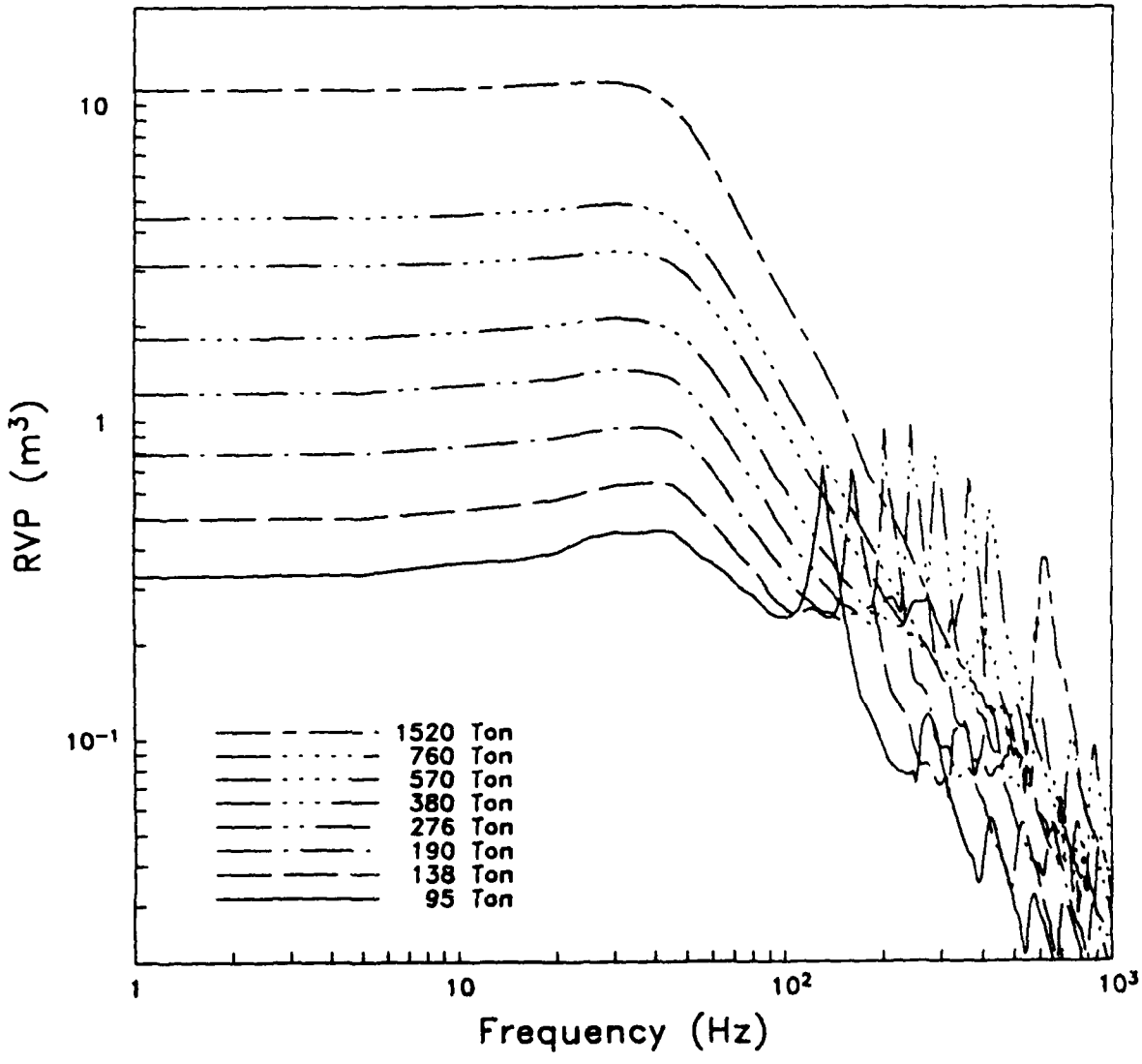

Figure 4.5. Reduced velocity potential for eight different yields for an air filled cavity inside a medium with a nonlinear salt material model.

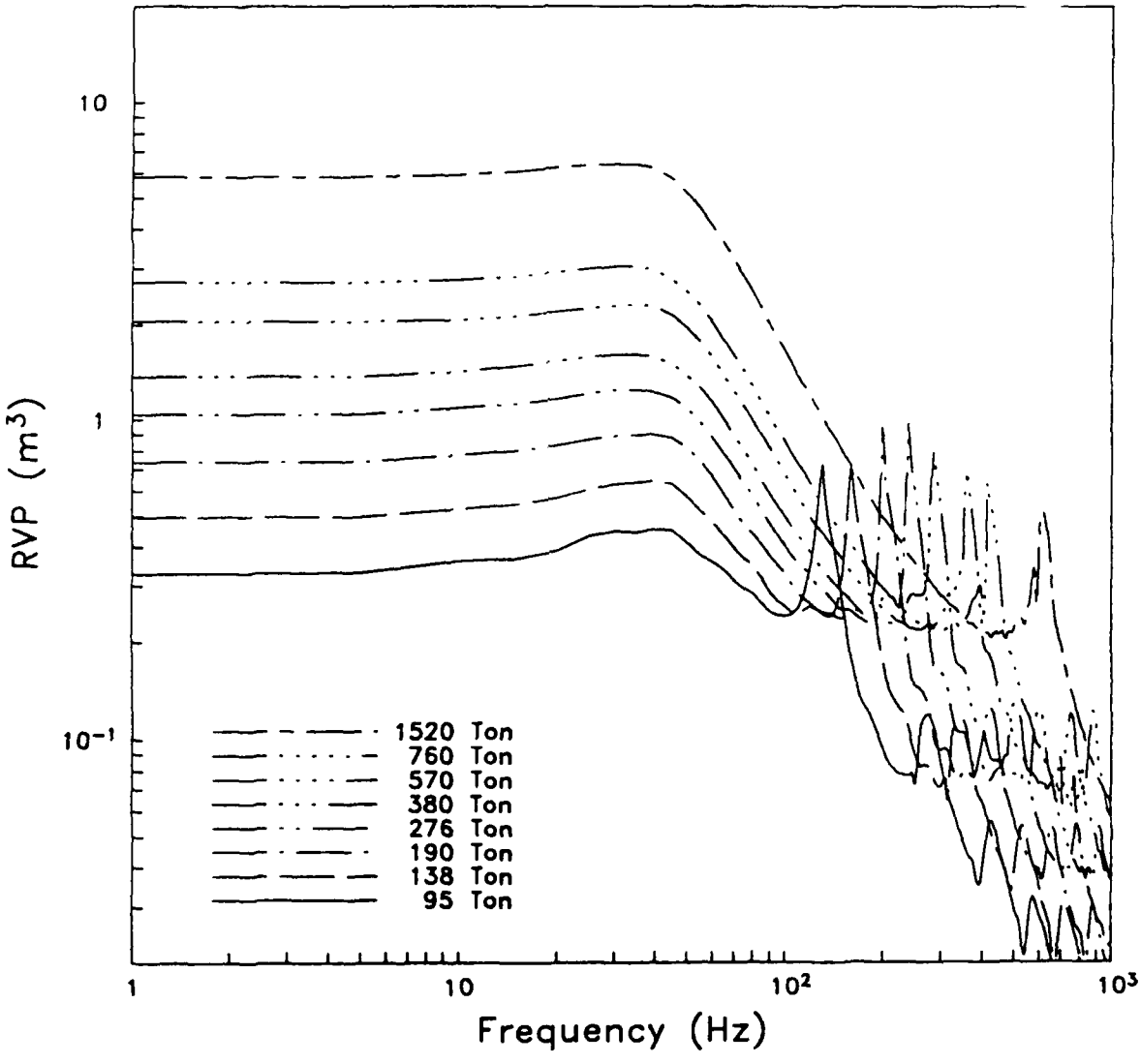

Figure 4.6. Reduced velocity potential for eight different yields for an air filled cavity inside a medium with a linear salt material model.

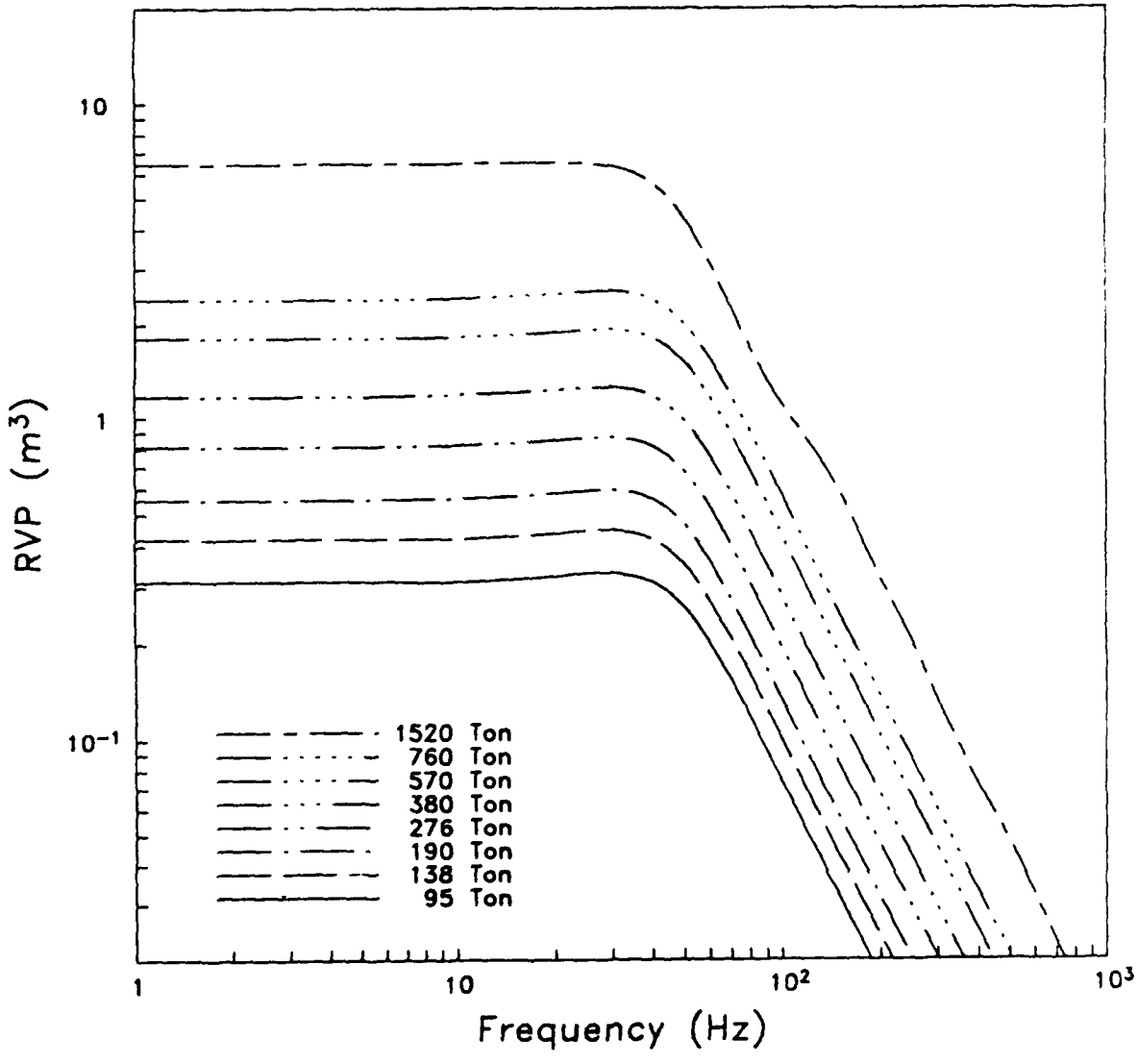

Figure 4.7. Reduced velocity potential for eight different yields for a step pressure on a cavity inside a medium with a nonlinear salt material model.

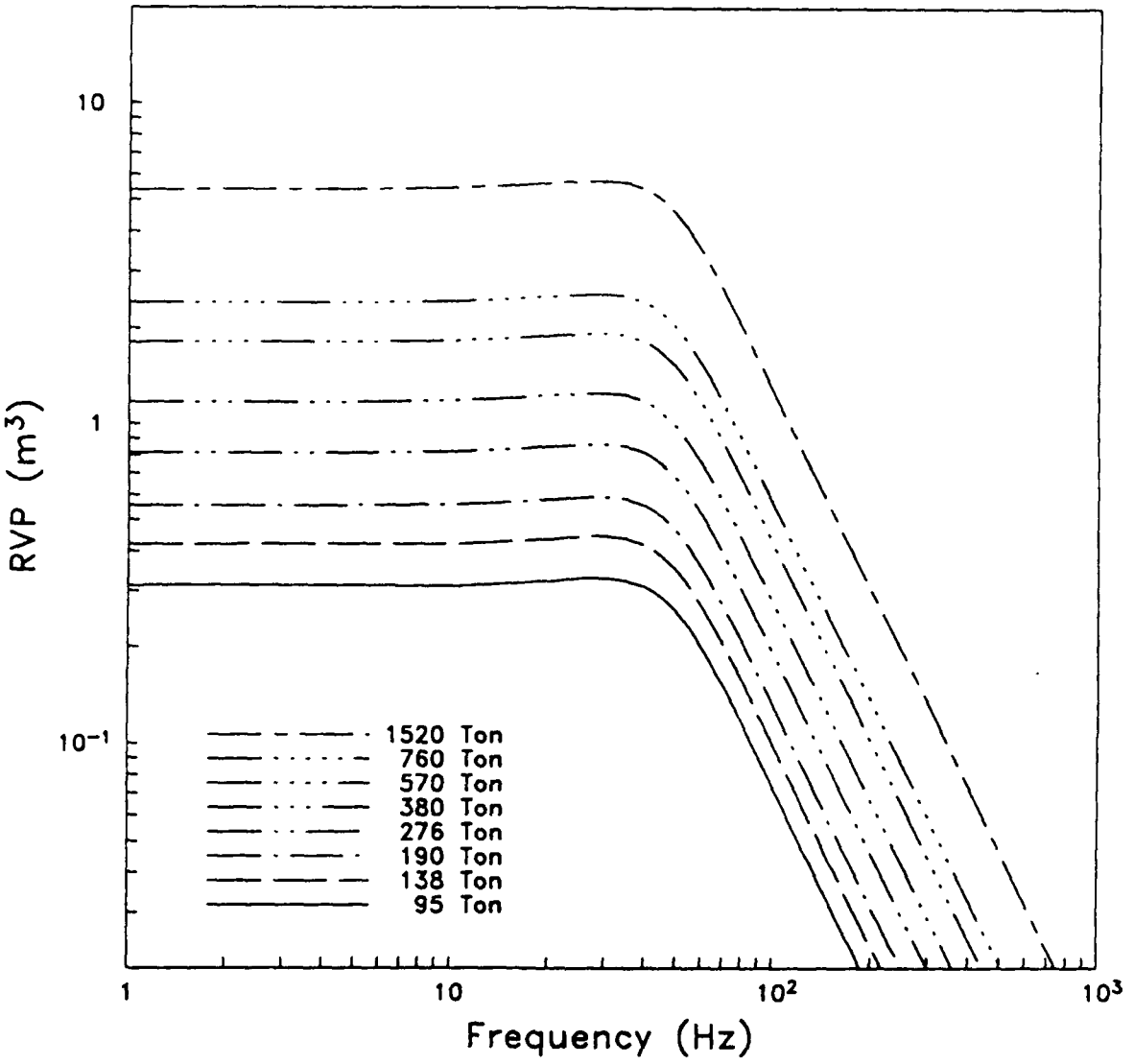

Figure 4.8. Reduced velocity potential for eight different yields for a step pressure on a cavity inside a medium with a linear salt material model.

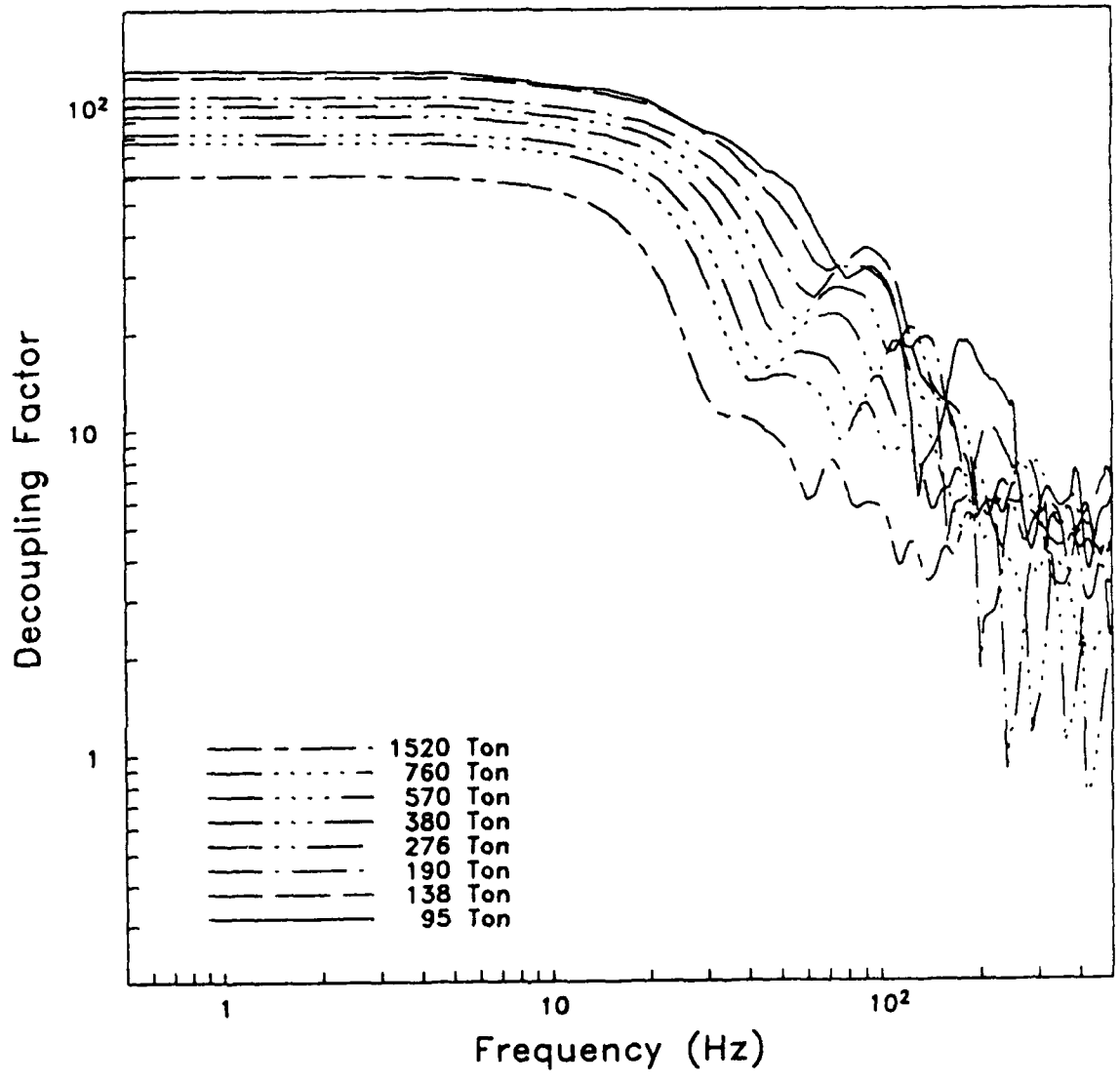

Figure 4.9. Frequency dependent decoupling factor for eight different yields for an air filled cavity inside a medium with a nonlinear salt material model.

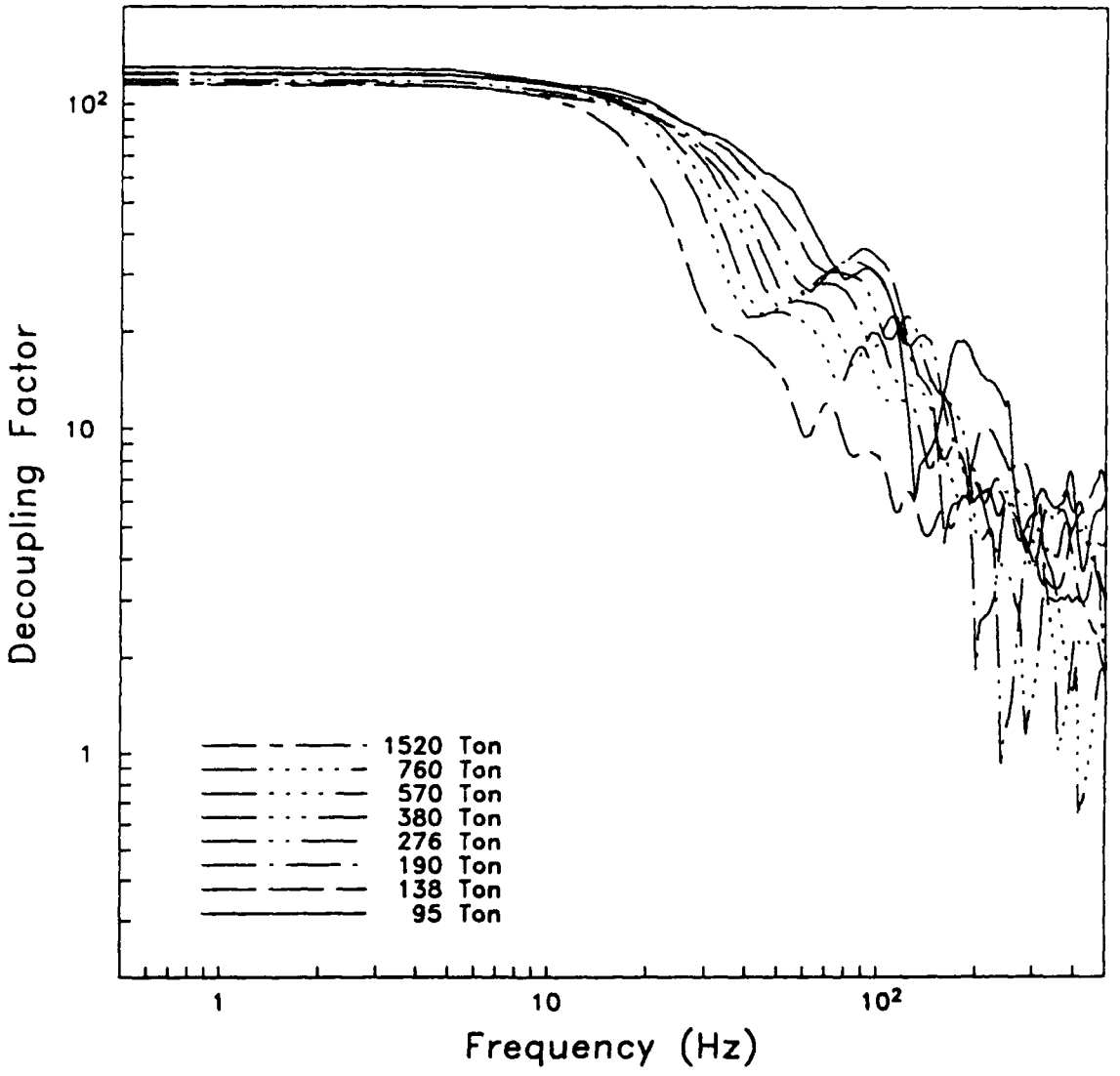

Figure 4.10. Frequency dependent decoupling factor for eight different yields for an air filled cavity inside a medium with a linear salt material model.

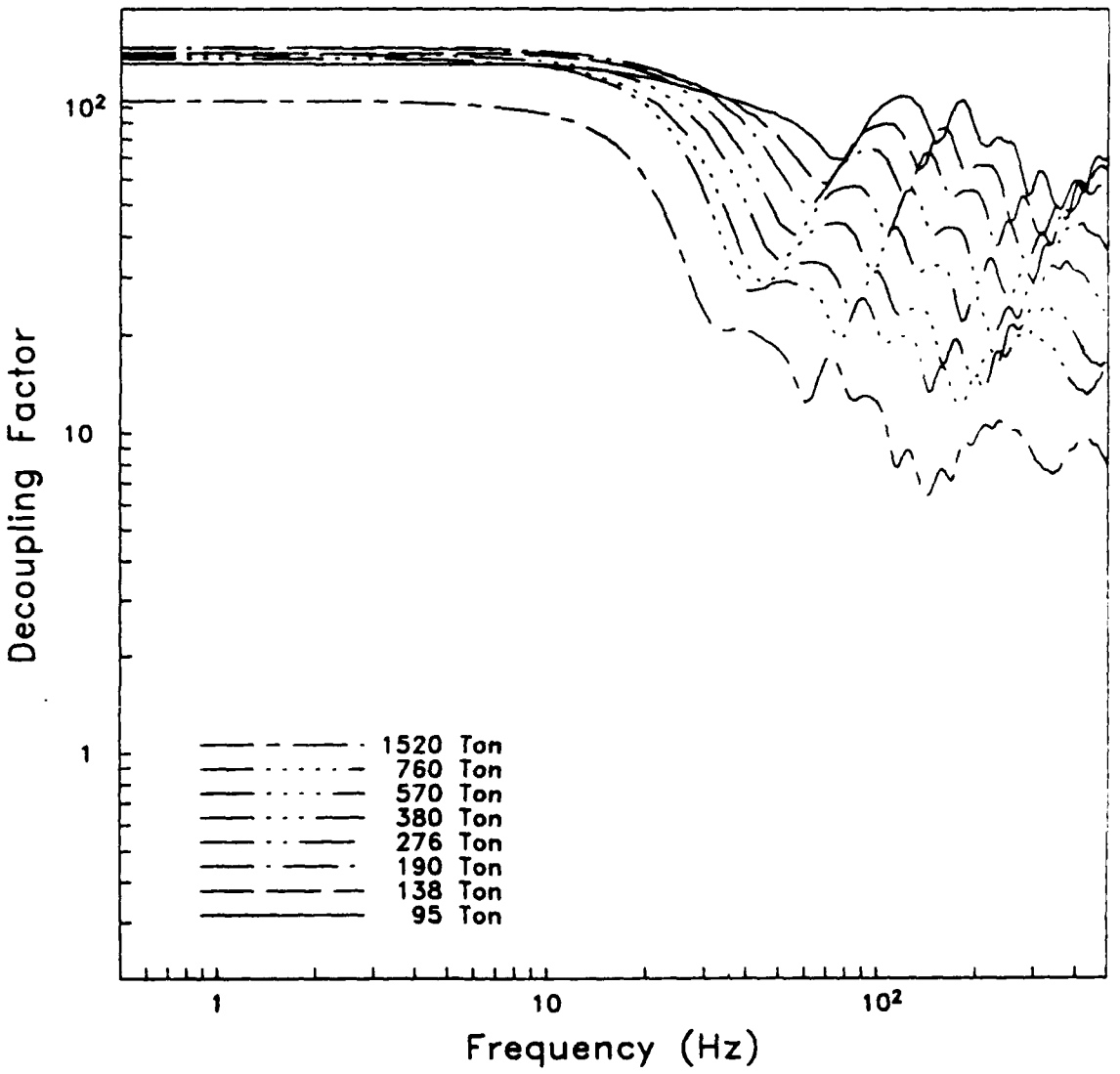

Figure 4.11. Frequency dependent decoupling factor for eight different yields for a step pressure on a cavity inside a medium with a nonlinear salt material model.

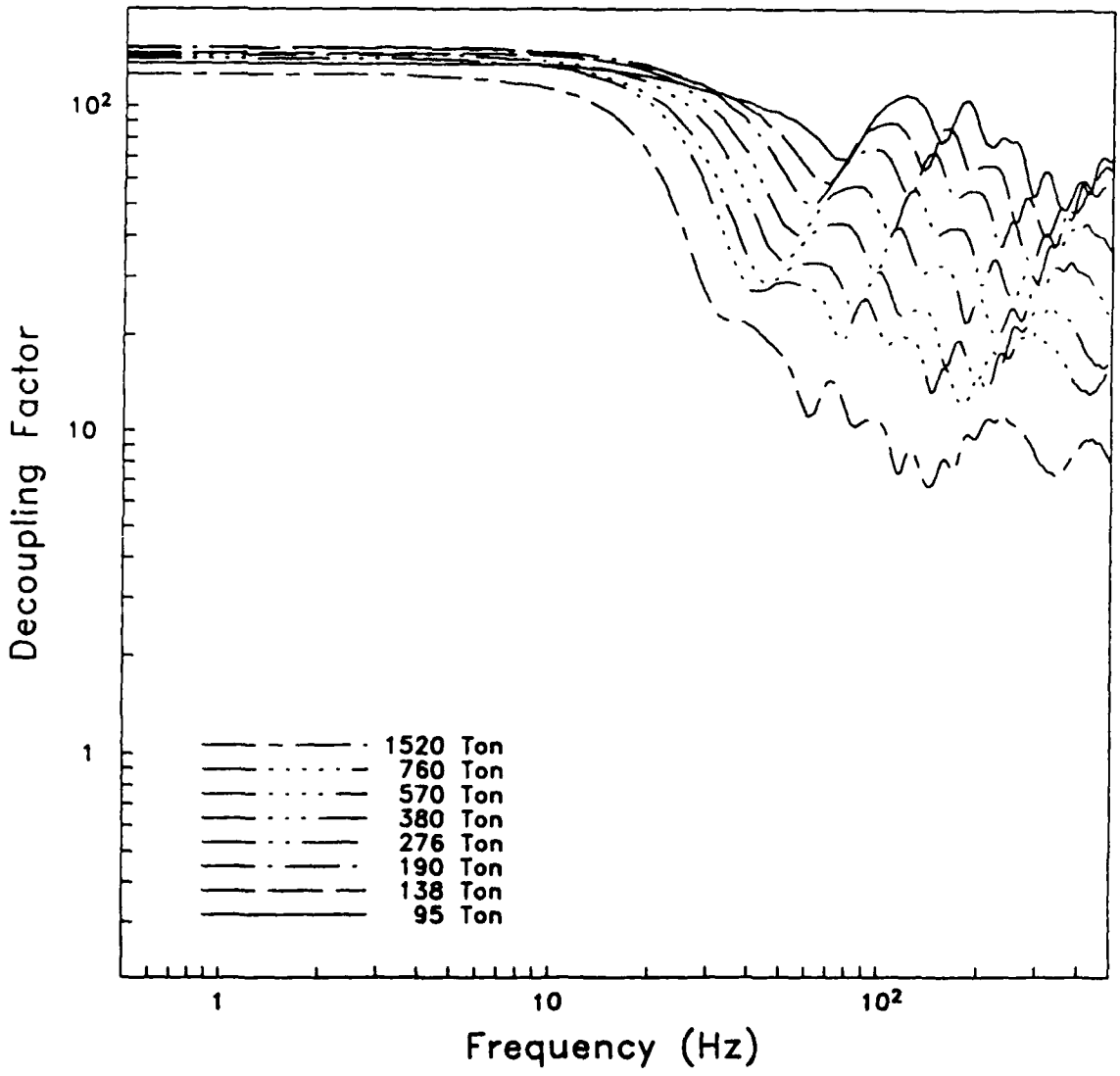

Figure 4.12. Frequency dependent decoupling factor for eight different yields for a step pressure on a cavity inside a medium with a linear salt material model.

5. DISCUSSION

An important result of this study is that we predict that a substantial amount of decoupling can be obtained using cavities that are significantly smaller than would be required for full decoupling. This result is consistent with earlier studies. For example, the OTA report (Office of Technology Assessment, 1988, Figure 6-4), shows that a 10 meter radius cavity is sufficient to decouple a one kiloton explosion to within about a factor of two of full decoupling, even though full decoupling would require a 25 meter radius cavity.

In this section we discuss three related topics: the implications of this result for detection of decoupled explosions; the possibility of discriminating decoupled explosions from other seismic sources because of spectral differences; and the stability of cavities used for detonating partially coupled explosions.

Rewriting the tables in the previous sections as a function of the ratio of yield W to the yield required for full decoupling W_f, we find the following low frequency decoupling factors (D) listed in Tables 5.1 and 5.2.

The significance of these results for evasion assessment can be envisioned more easily by considering m_b values which would be expected from explosions of different yields in cavities which span the range of sizes generally thought to be feasible (see, for example the 1988 OTA report). For purposes of illustration, we will assume that coupling in salt is comparable to that in competent rock media typified by that below the water table at NTS. An appropriate m_b/yield curve for such media has been reported by Murphy (1981) to be

$$m_b = 3.94 + 0.81 \log W . \qquad (5.1)$$

Similarly, it has been observed at NTS that for explosions in dry tuff, the observed m_b value for a given yield is lower than predicted by equation 5.1 by

TABLE 5.1

DECOUPLING FACTORS IN DRY TUFF

W/W_f	D	log D
0.95	44	1.64
1.91	36	1.55
2.86	32	1.50
3.81	29	1.45
7.62	19	1.27

TABLE 5.2

DECOUPLING FACTORS IN SALT

W/W_f	D	log D
0.86	83	1.92
1.25	76	1.88
1.73	72	1.86
2.59	62	1.79
3.45	59	1.77
6.91	47	1.67

0.5 to 1.0 magnitude units (Murphy, 1981). Taking 0.6 as a representative value, we obtain a corresponding NTS m_b/yield curve for dry tuff of the form

$$m_b = 3.34 - 0.81 \log W . \quad (5.2)$$

For explosions in the Soviet Union, it is generally believed that the m_b value for a given yield can be expected to be between 0.3 and 0.4 magnitude units greater than those given by Equations 5.1 and 5.2 (OTA, 1988). Adopting 0.3 as our nominal bias value, we then have for tamped explosions in Soviet salt

$$m_b = 4.24 - 0.81 \log W \quad (5.3)$$

and for tamped explosions in dry tuff

$$m_b = 3.64 - 0.81 \log W . \quad (5.4)$$

Making the reasonable assumption that the dependence of decoupling *effectiveness on* yield is independent of the absolute value of W_f (i. e. simple yield scaling is applicable), it is a straightforward matter to estimate the m_b/yield relations corresponding to explosions in different sized cavities. Thus, if m_b (T) denotes the m_b values corresponding to a fully tamped explosion of a given yield and m_b (D) denotes the m_b value corresponding to that same yield explosion in a particular sized cavity, then

$$m_b (D) = m_b (T) - \log D \quad (5.5)$$

where D is the decoupling factor appropriate for that value of W/W_f.

In Figures 5.1 and 5.2, we show the results of evaluating Equation 5.5 for cavities large enough to fully decouple 1 kiloton, 5 kiloton, and 10 kiloton explosions according to the Latter criterion. The figures show that if we adhere to the m_b 3.5 identification threshold quoted in the 1988 OTA report, decoupled explosions with yields on the order of 20 to 30 kilotons could evade identification, even if it were only possible to construct a cavity large enough to

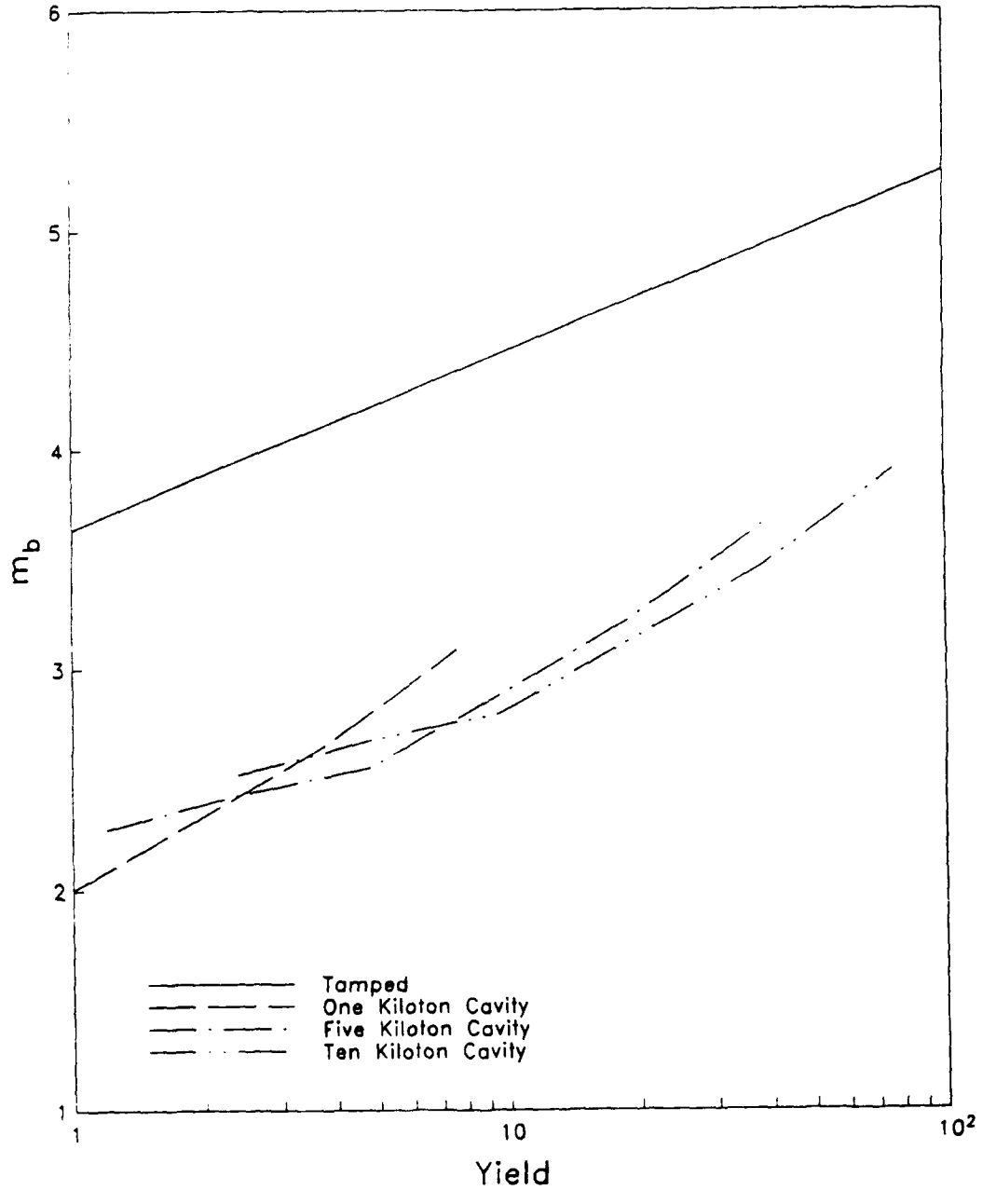

Figure 5.1. Predicted body wave magnitude for explosions in dry tuff. The four curves indicate the m_b for a tamped explosion, and m_b for explosions in cavities sufficient to decouple 1 KT, 5 KT, and 10 KT explosions.

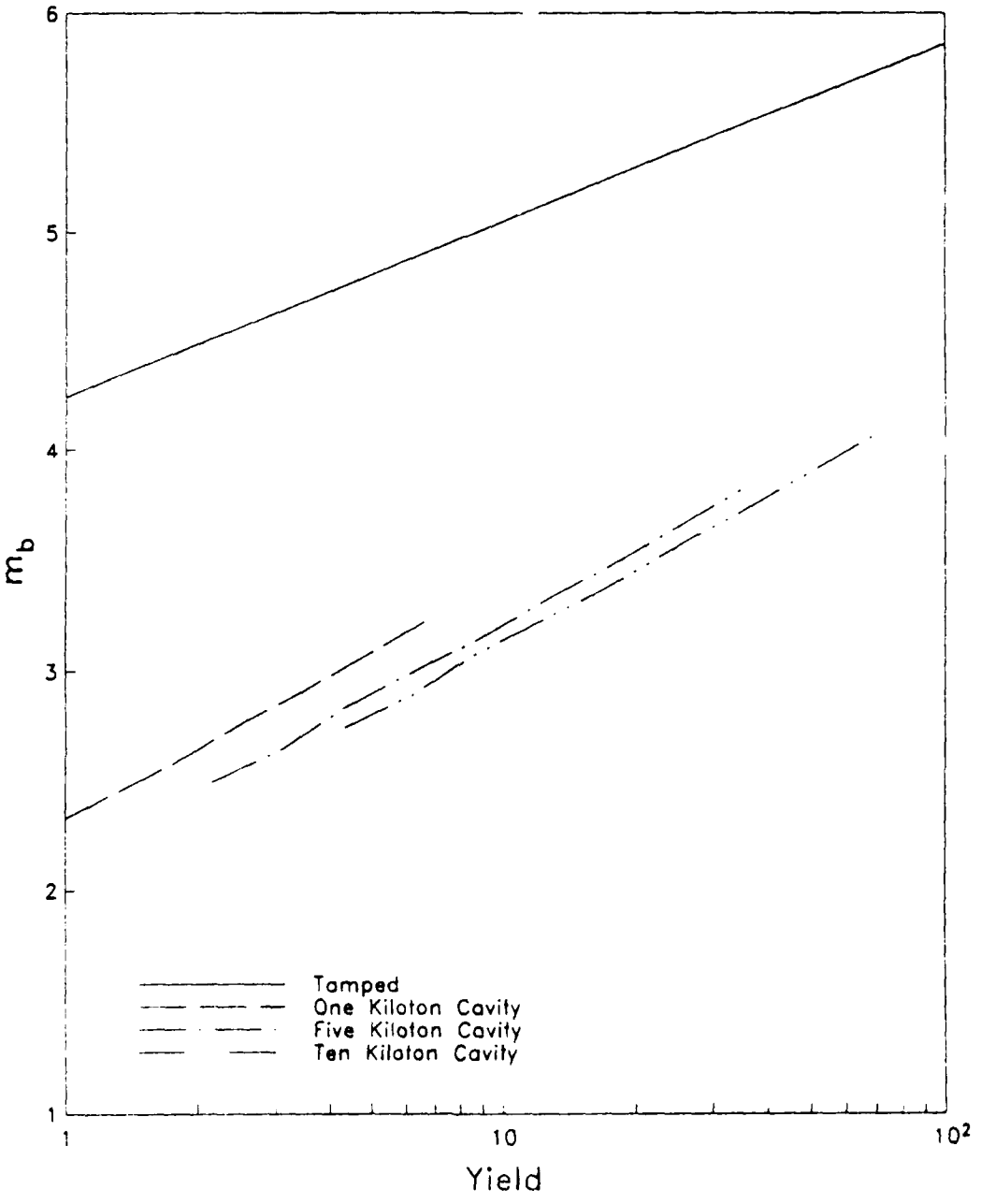

Figure 5.2. Predicted body wave magnitude for explosions in salt. The four curves indicate the m_b for a tamped explosion, and m_b for explosions in cavities sufficient to decouple 1 KT, 5 KT, and 10 KT explosions.

fully decouple 5 KT. In fact, the results shown in these figures suggest that it should be possible to detonate explosions with yields on the order of 10 KT in a cavity which is only large enough to fully decouple 1 KT and still remain well below the projected m_b 3.5 identification threshold.

Moving to the issue of discriminating decoupled explosions, we note that the spectra of decoupled explosions are distinctly different from tamped explosions because of the high frequency cavity oscillation peak. If this could be detected it might provide a way to discriminate a decoupled explosion from a small tamped explosion. Unfortunately, the peak occurs at very high frequency. In the examples shown in this report, the peaks all occur at frequencies greater than 100 Hz. The peak frequency will cube-root scale to lower frequencies for larger yields and cavity sizes. For a hypothetical fully decoupled 5 kiloton explosion in a 48 meter salt cavity, the spectral peak would occur at about 75 hz. This peak would be expected to occur at somewhat lower frequencies for overdecoupled explosions and at somewhat higher frequencies for partially decoupled explosions. However, it appears that in most cases of practical concern, it would occur in the high frequency band in which it has been found to be very difficult to separate source and propagation path effects (Murphy, *et al.*, 1988). It therefore seems unlikely that such spectral peaks could be reliably detected and identified at regional distances.

Finally, we want to mention the difficult issue of cavity stability. This is important for two reasons. First, an evader would have to be concerned about detection if a crater formed or radioactive products leaked from the explosion. Second, given the high cost of constructing such cavities, it would be advantageous if the cavities were reusable. There are a few observations that shed some light on this question. It is clear that cavity stability is strongly material dependent. Cavities resulting from tamped explosions in salt, for example (e.g. Salmon and Gnome), appear to be stable in general. On the other hand, cavities resulting from tamped or nearly tamped explosions in tuff nearly always collapse. For decoupled explosions in tuff, we know that smaller cavities are more likely to stand than larger cavities. Red Hot, which was substantially

overdriven collapsed. Diamond Dust and Diamond Mine, however, which were overdriven to a lesser degree, stayed open at least for the first 100 seconds after the explosion (whether or not they remained open to later times is unknown). Fully decoupled explosions in tuff, such as Mill Yard and Mini Jade, appear to be stable.

The current state of the art in numerical modeling is not adequate to definitively answer the question of cavity stability, particularly for late time collapses. The capability does exist, however, to assess the danger of hydrofracture, which is the most serious danger during and soon after cavity expansion and rebound.

The possibility of hydrofracture is increased when an event is partially decoupled by emplacement in a large underground cavity. Parametric ground motion calculations (Rimer, *et al.*, 1987) have shown that, for a tamped or nearly tamped event, cavity expansion, and subsequent dynamic inward motion (cavity rebound) which occurs within the first second, induce compressive residual hoop stresses in the rock surrounding the cavity which are much greater than the pressure of the radioactive cavity gases. (These stresses have been measured on both HE and nuclear events in tuff.) Thus, even if hydrofractures are initiated dynamically from the cavity during its outward expansion, the compressive hoop stresses developed during cavity rebound prevent these hydrofractures from propagating more than about one cavity radius from the wall of the expanded cavity. For somewhat more decoupled events, the smaller initial cavity pressure results in less cavity expansion but higher later time cavity pressure and lower residual stresses than for tamped event, thus increasing the hydrofracture possibility. Late time cavity pressure increases as decoupling is increased until only a small fraction of the device energy goes into cavity expansion. For larger initial cavities, residual stresses are negligible, and initial cavity pressure decreases with initial cavity size. For a fully decoupled event the cavity pressure is approximately equal to the in situ stress so that the hydrofracture threat is minimal.

S-CUBED has recently developed a capability to simultaneously model the dynamic ground motion and hydrofracture propagation. This capability (Rimer, *et al.*, 1987), (Nilson, *et al.*, 1987), called F-CUBED (Fast, Fluid, Fracture) models the fluid flow in the hydrofracture including loss mechanisms such as fluid friction, steam condensation, heat conduction and seepage into the walls of the fracture. These models have been applied to DNA nuclear events in tuff cavities, LANL events in alluvium cavities, and tamped LLNL events in complicated hard rock geologies on Pahute Mesa. Two examples of interest here are 0.5 and 2.0 kiloton overburied events in 11.0 m radius hemispheric cavities in a Rainier Mesa saturated zeolitic tuff geology. These events were overdriven by approximately factors of 24 and 95, respectively, which are considerably larger overdrives than were considered in the calculations in this report. For the 0.5 kiloton case, the calculated final cavity volume was about double its initial volume and a worst case single hydrofracture was calculated to propagate 210 m before stopping (depth of burial was approximately 400 m). The fracture stopped as a result of lowering of cavity pressure due to gas flow into the crack. If a discrete number of fractures out of the cavity were presumed, the fracture lengths would be significantly less due to greater cavity gas depletion. For the 2.0 KT case, the calculated final cavity volume was 11 times initial volume and the fracture propagated 281 m before ending in a very porous tuff layer above the working point. Although compressive residual stresses were calculated in this case, they were not large enough to prevent fracture propagation. These results are material dependent, with more brittle, stronger rock expected to induce greater hydrofracturing.

In the calculations done in this report, the final displacement of the cavity surface was 0.3 percent of the cavity radius for salt and 0.5 percent of the cavity radius in tuff for the largest cases of overdrive considered (approximately a factor of 8), and the final cavity volumes were increased by 10 percent and 15 percent respectively. Since the danger of hydrofracture would be considerably less than in the cases considered above, it would appear to be possible to construct cavities that could be overdriven by this amount in which the danger of hydrofracture, at least to the extent that detection would be a danger, could be minimized.

6. CONCLUSIONS

We have performed a series of nonlinear finite difference calculations to model explosions in air-filled cavities in salt and tuff media. The purpose of the study was to obtain an improved understanding of the seismic source function of decoupled, overdecoupled, and partially coupled explosions. The results of this set of simulations indicate that:

1. The low frequency decoupling level is strongly material dependent, and is a function of the shear modulus and tamped coupling of the medium and to a lesser extent a function of the air inside the cavity.

2. The amount of decoupling decreases slowly as yield is increased above the yield required for complete decoupling. In both the tuff and salt models used in this study, low frequency decoupling is reduced by only about a factor of two at an explosion yield eight times the Latter decoupling criterion. In fact, assuming that simple yield scaling is applicable, these calculational results suggest that it should be possible to decouple explosions with yields on the order of 20 to 30 kilotons in a cavity large enough to fully decouple only 5 kilotons and still remain below the m_b 3.5 identification threshold cited in the recent 1988 OTA report on seismic monitoring.

3. Although the current state-of-the-art in numerical modeling is not adequate to definitively address the question of cavity stability, available calculational results for induced fracturing and limited test data do not seem to suggest that cavity stability should be a limiting factor for the range of cavity overdrive factors considered in this report.

4. In salt cavities, plastic flow begins at about the yield predicted by the Latter criterion. However, as mentioned above, the amount of decoupling decreases slowly with increasing explosion yield.

5. Explosions in cavities in unsaturated tuff decouple more than would be predicted based on linear theory. This happens because the dominant nonlinear mechanism which is operating at low stress levels is pore crushing which attenuates the outgoing wave. A secondary result of this is that in tuff the decoupling factor decreases to less than one at sufficiently high frequencies. At sufficiently high explosion yields, about a factor of five higher than the Latter criterion, plastic flow becomes the dominant mechanism, and decoupling decreases to less than predicted by elastic theory.

6. The decoupling factor decreases at high frequencies, however this decrease occurs at higher frequency for lower yield events. Because of this, high frequency decoupling factors are larger for overdecoupled explosions than for "fully" decoupled explosions at the same frequency with the same cavity geometry.

7. At high frequencies, there is little difference between the source functions predicted by linear theory and those predicted by a nonlinear external material model, except for the effects of attenuation due to pore crushing in tuff. This happens because the high frequency spectra are dominated by cavity reverberations. This is true for overdecoupled, decoupled, and partially coupled explosions.

7. REFERENCES

Evernden, J. F., C. B. Archambeau and E. Cranswick (1986), "An Evaluation of Seismic Decoupling and Underground Nuclear Explosion Test Monitoring Using High Frequency Seismic Data", Reviews of *Geophysics, 24,* pp. 143-215.

Heard, H. C., A. E. Abey, B. P. Bonner and A. Duba (1975), "Stress-Strain Behavior of Polycrystalline NACL to 3.2 GPa", Lawrence Livermore Laboratory Report, UCRL-51743.

Latter, A. L., R. E. Lelevier, E. A. Martinelli and W. G. McMillan (1961), "A Method of Concealing Underground Nuclear Explosions," *J. Geophys. Res., 66,* p. 2929.

Murphy, J. R. (1981), "P Wave Coupling of Underground Explosions in Various Geologic Media", in *Identification of Seismic Sources - Earthquake or Underground Explosion*, Proc. of NATO ASI, E. Husebye and S. Mykkeltveit, Editors, Riedel Publishing Co. Dordrecht, Holland, pp. 201-205.

Murphy, J. R., J. L. Stevens and N. Rimer (1988), "High Frequency Seismic Source Characteristics of Cavity Decoupled Underground Nuclear Explosions," S-CUBED Topical Report to the Air Force Geophysics Laboratory, AFGL-TR-88-0130, SSS-R-88-9595, May. ADA198121

Nilson, R. H., N. Rimer and E. J. Halda (1987), "Simultaneous Modeling of Dynamic Ground Motion and Fluid Flow in Hydrofractures," Proceedings of the Fourth Containment Symposium on Underground Nuclear Explosions, (at U. S. Air Force Academy, Colorado Springs, Colorado, September 1987). Published by Sandia National Laboratories, Conference-870961.

Office of Technology Assessment (1988), "Seismic Verification of Nuclear Testing Treaties", OTA-ISC-361 (Washington, D. C.: U.S. Government Printing Office, May 1988).

Patterson, D. W. (1964), "Theory of Nuclear Explosion in a Cavity Including the Effects of Shock and Nonelastic Effects on the Wall and Comparison With Tamped Explosions - Project Dribble, Lawrence Radiation Laboratory Report UCRL-7916, June.

Rimer, N. and J. T. Cherry (1982), "Ground Motion Predictions for the Grand Saline Experiment," S-CUBED Topical Report to VELA Seismological Center, SSS-R-82-5673, VSC-TR-82-25, July.

Rimer, N., E. J. Halda, K. H. Lie and R. H. Nilson (1987), "Containment Analysis for the Mission Ghost Cavity Event," Proceedings of the Fourth Containment Symposium on Underground Nuclear Explosions, (at U. S. Air Force Academy, Colorado Springs, Colorado, September 1987). Published by Sandia National Laboratories, Conference-870961.

Rimer, N., R. H. Nilson, E. J. Halda and K. H. Lie (1987), "Recent Developments in Hydrofracture Calculations Related to Containment," Proceedings of the Fourth Containment Symposium on Underground Nuclear Explosions, (at U. S. Air Force Academy, Colorado Springs, Colorado, September 1987). Published by Sandia National Laboratories, Conference-870961.

Stevens, J. L. and S. M. Day (1985), "The Physical Basis of the m_b:M_s and Variable Frequency Magnitude Methods for Earthquake/Explosion Discrimination," *Journal of Geophysical Research, v. 90,* pp. 3009-3020.

CONTRACTORS (United States)

Professor Keiiti Aki
Center for Earth Sciences
University of Southern California
University Park
Los Angeles, CA 90089-0741

Professor Thomas Ahrens
Seismological Lab, 252-21
Div. of Geological & Planetary Sci.
California Institute of Technology
Pasadena, CA 91125

Professor Charles B. Archambeau
Cooperative Institute for Resch
in Environmental Sciences
University of Colorado
Boulder, CO 80309

Dr. Thomas C. Bache Jr.
Science Applications Int'l Corp.
10210 Campus Point Drive
San Diego, CA 92121 (2 copies)

Dr. Muawia Barazangi
Institute for the Study of
of the Continent
Cornell University
Ithaca, NY 14853

Dr. Douglas R. Baumgardt
Signal Analysis & Systems Div.
ENSCO, Inc.
5400 Port Royal Road
Springfield, VA 22151-2388

Dr. Jonathan Berger
IGPP, A-205
Scripps Institution of Oceanography
University of California, San Diego
La Jolla, CA 92093

Dr. S. Bratt
Science Applications Int'l Corp.
10210 Campus Point Drive
San Diego, CA 92121

Dr. Lawrence J. Burdick
Woodward-Clyde Consultants
P.O. Box 93245
Pasadena, CA 91109-3245 (2 copies)

Professor Robert W. Clayton
Seismological Laboratory/Div. of
Geological & Planetary Sciences
California Institute of Technology
Pasadena, CA 91125

Dr Karl Coyner
New England Research, Inc.
76 Olcott Drive
White River Junction, VT 05001

Dr. Vernon F. Cormier
Department of Geology & Geophysics
U-45, Room 207
The University of Conneticut
Storrs, Connecticut 06268

Dr. Steven Day
Dept. of Geological Sciences
San Diego State U.
San Diego, CA 92182

Dr. Zoltan A. Der
ENSCO, Inc.
5400 Port Royal Road
Springfield, VA 22151-2388

Professor John Ferguson
Center for Lithospheric Studies
The University of Texas at Dallas
P.O. Box 830688
Richardson, TX 75083-0688

Professor Stanley Flatte'
Applied Sciences Building
University of California,
Santa Cruz, CA 95064

Dr. Alexander Florence
SRI International
333 Ravenswood Avenue
Menlo Park, CA 94025-3493

Professor Steven Grand
University of Texas at Austin
Dept of Geological Sciences
Austin, TX 78713-7909

Dr. Henry L. Gray
C.F. Frensley Professor of Mathematics
& Statistics, Vice Provost and Dean
Department of Statistical Sciences
Southern Methodist University
Dallas, TX 75275

Professor Roy Greenfield
Geosciences Department
403 Deike Building
The Pennsylvania State University
University Park, PA 16802

Dr. Indra N. Gupta
Teledyne Geotech
314 Montgomery St.
Alexandria, VA 22314

Professor David G. Harkrider
Seismological Laboratory
Div of Geological & Planetary Sciences
California Institute of Technology
Pasadena, CA 91125

Professor Donald V. Helmberger
Seismological Laboratory
Div of Geological & Planetary Sciences
California Institute of Technology
Pasadena, CA 91125

Professor Eugene Herrin
Institute for the Study of Earth
and Man/Geophysical Laboratory
Southern Methodist University
Dallas, TX 75275

Professor Robert B. Herrmann
Department of Earth & Atmospheric
Sciences
Saint Louis University
Saint Louis, MO 63156

Professor Bryan Isacks
Cornell University
Dept of Geological Sciences
SNEE Hall
Ithaca, NY 14850

Professor Lane R. Johnson
Seismographic Station
University of California
Berkeley, CA 94720

Professor Thomas H. Jordan
Department of Earth, Atmospheric
and Planetary Sciences
Mass Institute of Technology
Cambridge, MA 02139

Dr. Alan Kafka
Department of Geology &
Geophysics
Boston College
Chestnut Hill, MA 02167

Professor Leon Knopoff
University of California
Institute of Geophysics
& Planetary Physics
Los Angeles, CA 90024

Professor Charles A. Langston
Geosciences Department
403 Deike Building
The Pennsylvania State University
University Park, PA 16802

Professor Thorne Lay
Department of Geological Sciences
1006 C.C. Little Building
University of Michigan
Ann Arbor, MI 48109-1063

Dr. Randolph Martin III
New England Research, Inc.
76 Olcott Drive
White River Junction, VT 05001

Dr. Gary McCartor
Mission Research Corp.
735 State Street
P.O. Drawer 719
Santa Barbara, CA 93102 (2 copies)

Professor Thomas V. McEvilly
Seismographic Station
University of California
Berkeley, CA 94720

Dr. Keith L. McLaughlin
S-CUBED,
A Division of Maxwell Laboratory
P.O. Box 1620
La Jolla, CA 92038-1620

Professor William Menke
Lamont-Doherty Geological Observatory
of Columbia University
Palisades, NY 10964

Dr. Bernard Minster
IGPP, A-205
Scripps Institute of Oceanography
Univ. of California, San Diego
La Jolla, CA 92093

Professor Brian J. Mitchell
Department of Earth & Atmospheric
Sciences
Saint Louis University
Saint Louis, MO 63156

Mr. Jack Murphy
S-CUBED, A Division of Maxwell Lab
11800 Sunrise Valley Drive
Suite 1212
Reston, VA 22091 (2 copies)

Dr. Bao Nguyen
GL/LWH
Hanscom AFB, MA 01731-5000

Professor J. A. Orcutt
IGPP, A-205
Scripps Institute of Oceanography
Univ. of California, San Diego
La Jolla, CA 92093

Professor Keith Priestley
University of Nevada
Mackay School of Mines
Reno, NV 89557

Professor Paul G. Richards
Lamont-Doherty Geological
Observatory of Columbia Univ.
Palisades, NY 10964

Wilmer Rivers
Teledyne Geotech
314 Montgomery Street
Alexandria, VA 22314

Dr. Alan S. Ryall, Jr.
Center of Seismic Studies
1300 North 17th Street
Suite 1450
Arlington, VA 22209-2308 (4 copies)

Professor Charles G. Sammis
Center for Earth Sciences
University of Southern California
University Park
Los Angeles, CA 90089-0741

Professor Christopher H. Scholz
Geological Sciences
Lamont-Doherty Geological Observatory
Palisades, NY 10964

Dr. Jeffrey L. Stevens
S-CUBED,
A Division of Maxwell Laboratory
P.O. Box 1620
La Jolla, CA 92038-1620

Professor Brian Stump
Institute for the Study of Earth & Man
Geophysical Laboratory
Southern Methodist University
Dallas, TX 75275

Professor Ta-Liang Teng
Center for Earth Sciences
University of Southern California
University Park
Los Angeles, CA 90089-0741

Dr. Clifford Thurber
University of Wisconsin - Madison
Dept. of Geology & Geophysics
1215 West Dayton St.
Madison, WS 53706

Professor M. Nafi Toksoz
Earth Resources Lab
Massachusetts Institute of Technology
42 Carleton Street
Cambridge, MA 02142

Professor Terry C. Wallace
Department of Geosciences
Building #77
University of Arizona
Tucson, AZ 85721

Weidlinger Associates
ATTN: Dr. Gregory Wojcik
4410 El Camino Real, Suite 110
Los Altos, CA 94022

Ray Willeman
GL/LWH
Hanscom AFB, MA 01731-5000

Dr. Lorraine Wolfe
GL/LWH
Hanscom AFB, MA 01731-5000

Professor Francis T. Wu
Department of Geological Sciences
State University of New York
at Binghamton
Vestal, NY 13901

OTHERS (United States)

Dr. Monem Abdel-Gawad
Rockwell Internat'l Science Center
1049 Camino Dos Rios
Thousand Oaks, CA 91360

Professor Shelton S. Alexander
Geosciences Department
403 Deike Building
The Pennsylvania State University
University Park, PA 16802

Dr. Ralph Archuleta
Department of Geological Sciences
Univ. of California at
Santa Barbara
Santa Barbara, CA

J. Barker
Department of Geological Sciences
State University of New York
at Binghamton
Vestal, NY 13901

Mr. William J. Best
907 Westwood Drive
Vienna, VA 22180

Dr. N. Biswas
Geophysical Institute
University of Alaska
Fairbanks, AK 99701

Dr. G. A. Bolling
Department of Geological Sciences
Virginia Polytechnical Institute
21044 Derring Hall
Blacksburg, VA 24061

Mr. Roy Burger
1221 Serry Rd.
Schenectady, NY 12309

Dr. Robert Burridge
Schlumberger-Doll Resch Ctr.
Old Quarry Road
Ridgefield, CT 06877

Science Horizons, Inc.
ATTN: Dr. Theodore Cherry
710 Encinitas Blvd., Suite 200
Encinitas, CA 92024 (2 copies)

Professor Jon F. Claerbout
Professor Amos Nur
Dept. of Geophysics
Stanford University
Stanford, CA 94305 (2 copies)

Dr. Anton W. Dainty
Earth Resources Lab
Massachusetts Institute of Technology
42 Carleton Street
Cambridge, MA 02142

Professor Adam Dziewonski
Hoffman Laboratory
Harvard University
20 Oxford St.
Cambridge, MA 02138

Professor John Ebel
Dept of Geology and Geophysics
Boston College
Chestnut Hill, MA 02167

Dr. Donald Forsyth
Dept of Geological Sciences
Brown University
Providence, RI 02912

Dr. Anthony Gangi
Texas A&M University
Department of Geophysics
College Station, TX 77843

Dr. Freeman Gilbert
Inst. of Geophysics & Planetary Physics
University of California, San Diego
P.O. Box 109
La Jolla, CA 92037

Mr. Edward Giller
Pacific Seirra Research Corp.
1401 Wilson Boulevard
Arlington, VA 22209

Dr. Jeffrey W. Given
Sierra Geophysics
11255 Kirkland Way
Kirkland, WA 98033

Rong Song Jih
Teledyne Geotech
314 Montgomery Street
Alexandria, VA 22314

Professor F.K. Lamb
Univ. of Illinois at Urbana-Champaign
Department of Physics
1110 West Green Street
Urbana, IL 61801

Dr. Arthur Lerner-Lam
Lamont-Doherty Geological Observatory
of Columbia University
Palisades, NY 10964

Dr. L. Timothy Long
School of Geophysical Sciences
Georgia Institute of Technology
Atlanta, GA 30332

Dr. Peter Malin
University of California at
Santa Barbara
Institute for Central Studies
Santa Barbara, CA 93106

Dr. George R. Mellman
Sierra Geophysics
11255 Kirkland Way
Kirkland, WA 98033

Professor John Nabelek
College of Oceanography
Oregon State University
Corvallis, OR 97331

Dr. Geza Nagy
U. California, San Diego
Dept of Ames, M.S. B-010
La Jolla, CA 92093

Dr. Jack Oliver
Department of Geology
Cornell University
Ithaca, NY 14850

Dr. Robert Phinney/Dr. F. A. Dahlen
Dept of Geological
Geological Science University
Princeton University
Princeton, NJ 08540

RADIX System, Inc.
Attn: Dr. Jay Pulli
2 Taft Court, Suite 203
Rockville, Maryland 20850

Dr. Norton Rimer
S-CUBED
A Division of Maxwell Laboratory
P.O. 1620
La Jolla, CA 92038-1620

Professor Larry J. Ruff
Department of Geological Sciences
1006 C.C. Little Building
University of Michigan
Ann Arbor, MI 48109-1063

Dr. Richard Sailor
TASC Inc.
55 Walkers Brook Drive
Reading, MA 01867

Thomas J. Sereno, Jr.
Science Application Int'l Corp.
10210 Campus Point Drive
San Diego, CA 92121

Dr. David G. Simpson
Lamont-Doherty Geological Observ.
of Columbia University
Palisades, NY 10964

Dr. Bob Smith
Department of Geophysics
University of Utah
1400 East 2nd South
Salt Lake City, UT 84112

Dr. S. W. Smith
Geophysics Program
University of Washington
Seattle, WA 98195

Dr. Stewart Smith
IRIS Inc.
1616 N. Fort Myer Dr.
Suite 1440
Arlington, VA 22209

Rondout Associates
ATTN: Dr. George Sutton,
Dr. Jerry Carter, Dr. Paul Pomeroy
P. O. Box 224
Stone Ridge, NY 12484 (4 copies)

Dr. L. Sykes
Lamont Doherty Geological Observ.
Columbia University
Palisades, NY 10964

Dr. Pradeep Talwani
Department of Geological Sciences
University of South Carolina
Columbia, SC 29208

Dr. R. B. Tittmann
Rockwell International Science Center
1049 Camino Dos Rios
P.O. Box 1085
Thousand Oaks, CA 91360

Dr. Gregory van der Vink
IRIS, Inc.
1616 No. Fort Myer Drive
Suite 1440
Arlington, VA 22209

Professor John H. Woodhouse
Hoffman Laboratory
Harvard University
20 Oxford St.
Cambridge, MA 02138

Dr. Gregory B. Young
ENSCO, Inc.
5400 Port Royal Road
Springfield, VA 22151-2388

FOREIGN (OTHERS)

Dr. Peter Basham
Earth Physics Branch
Geological Survey of Canada
1 Observatory Crescent
Ottawa, Ontario, CANADA K1A 0Y3

Professor Ari Ben-Menahem
Dept of Applied Mathematics
Weizman Institute of Science
Rehovot
ISRAEL 951729

Dr. Eduard Berg
Institute of Geophysics
University of Hawaii
Honolulu, HI 96822

Dr. Michel Bouchon
I.R.I.G.M-B.P.
38402 St. Martin D'Heres
Cedex FRANCE

Dr. Hilmar Bungum/NTNF/NORSAR
P.O. Box 51
Norwegian Council of Science,
Industry and Research, NORSAR
N-2007 Kjeller, NORWAY

Dr. Michel Campillo
I.R.I.G.M.-B.P. 68
38402 St. Martin D'Heres
Cedex, FRANCE

Dr. Kin-Yip Chun
Geophysics Division
Physics Department
University of Toronto
Ontario, CANADA M5S 1A7

Dr. Alan Douglas
Ministry of Defense
Blacknest, Brimpton,
Reading RG7-4RS
UNITED KINGDOM

Dr. Manfred Henger
Fed. Inst. For Geosciences & Nat'l Res.
Postfach 510153
D-3000 Hannover 51
FEDERAL REPUBLIC OF GERMANY

Ms. Eva Johannisson
Senior Research Officer
National Defense Research Inst.
P.O. Box 27322
S-102 54 Stockholm, SWEDEN

Tormod Kvaerna
NTNF/NORSAR
P.O. Box 51
N-2007 Kjeller, NORWAY

Mr. Peter Marshall, Procurement
Executive, Ministry of Defense
Blacknest, Brimpton,
Reading FG7-4RS
UNITED KINGDOM (3 copies)

Dr. Robert North
Geophysics Division
Geological Survey of Canada
1 Observatory crescent
Ottawa, Ontario, CANADA K1A 0Y3

Dr. Frode Ringdal
NTNF/NORSAR
P.O. Box 51
N-2007 Kjeller, NORWAY

Dr. Jorg Schlittenhardt
Fed. Inst. for Geosciences & Nat'l Res.
Postfach 510153
D-3000 Hannover 51
FEDERAL REPUBLIC OF GERMANY

University of Hawaii
Institute of Geophysics
ATTN: Dr. Daniel Walker
Honolulu, HI 96822

FOREIGN CONTRACTORS

Dr. Ramon Cabre, S.J.
Observatorio San Calixto
Casilla 5939
La Paz Bolivia

Professor Peter Harjes
Institute for Geophysik
Rhur University/Bochum
P.O. Box 102148, 4630 Bochum 1
FEDERAL REPUBLIC OF GERMANY

Dr. E. Husebye
NTNF/NORSAR
P.O. Box 51
N-2007 Kjeller, NORWAY

Professor Brian L.N. Kennett
Research School of Earth Sciences
Institute of Advanced Studies
G.P.O. Box 4
Canberra 2601, AUSTRALIA

Dr. B. Massinon
Societe Radiomana
27, Rue Claude Bernard
75005, Paris, FRANCE (2 copies)

Dr. Pierre Mechler
Societe Radiomana
27, Rue Claude Bernard
75005, Paris, FRANCE

Dr. Svein Mykkeltveit
NTNF/NORSAR
P.O. Box 51
N-2007 Kjeller, NORWAY (3 copies)

GOVERNMENT

Dr. Ralph Alewine III
DARPA/NMRO
1400 Wilson Boulevard
Arlington, VA 22209-2308

James C. Battis
GL/LWH
Hanscom AFB, MA 01731-5000

Dr. Robert Blandford
DARPA/NMRO
1400 Wilson Boulevard
Arlington, VA 22209-2308

Dr. John J. Cipar
GL/LWH
Hanscom AFB, MA 01731-5000

Sandia National Laboratory
ATTN: Dr. H. B. Durham
Albuquerque, NM 87185

Dr. Jack Evernden
USGS-Earthquake Studies
345 Middlefield Road
Menlo Park, CA 94025

U.S. Geological Survey
ATTN: Dr. T. Hanks
Nat'l Earthquake Resch Center
345 Middlefield Road
Menlo Park, CA 94025

Dr. James Hannon
Lawrence Livermore Nat'l Lab.
P.O. Box 808
Livermore, CA 94550

Paul Johnson
ESS-4, Mail Stop J979
Los Alamos National Laboratory
Los Alamos, NM 87545

Janet Johnston
GL/LWH
Hanscom AFB, MA 01731-5000

Dr. Katherine Kadinsky-Cade
GL/LWH
Hanscom AFB, MA 01731-5000

Ms. Ann Kerr
IGPP, A-205
Scripps Institute of Oceanography
Univ. of California, San Diego
La Jolla, CA 92093

Dr. Max Koontz
US Dept of Energy/DP 5
Forrestal Building
1000 Independence Ave.
Washington, D.C. 20585

Dr. W. H. K. Lee
Office of Earthquakes, Volcanoes,
& Engineering
345 Middlefield Rd
Menlo Park, CA 94025

Dr. William Leith
U.S. Geological Survey
Mail Stop 928
Reston, VA 22092

Dr. Richard Lewis
Dir. Earthquake Engrg & Geophysics
U.S. Army Corps of Engineers
Box 631
Vicksburg, MS 39180

James F. Lewkewicz
GL/LWH
Hanscom AFB, MA 01731-5000

Stephen Mangino
GL/LWH
Hanscom AFB, MA 01731-5000

Dr. Robert Masse'
Box 25046, Mail Stop 967
Denver Federal Center
Denver, CO 80225

Richard Morrow
ACDA/VI
Room 5741
320 21st Street N.W.
Washington, D.C. 20451

Dr. Keith K. Nakanishi
Lawrence Livermore National Laboratory
P.O. Box 808, L-205
Livermore, CA 94550 (2 copies)

Dr. Carl Newton
Los Alamos National Lab.
P.O. Box 1663
Mail Stop C335, Group ESS-3
Los Alamos, NM 87545

Dr. Kenneth H. Olsen
Los Alamos Scientific Lab.
P.O. Box 1663
Mail Stop C335, Group ESS-3
Los Alamos, NM 87545

Howard J. Patton
Lawrence Livermore National Laboratory
P.O. Box 808, L-205
Livermore, CA 94550

Mr. Chris Paine
Office of Senator Kennedy
SR 315
United States Senate
Washington, D.C. 20510

AFOSR/NP
ATTN: Colonel Jerry J. Perrizo
Bldg 410
Bolling AFB, Wash D.C. 20332-6448

HQ AFTAC/TT
Attn: Dr. Frank F. Pilotte
Patrick AFB, Florida 32925-6001

Mr. Jack Rachlin
USGS - Geology, Rm 3 C136
Mail Stop 928 National Center
Reston, VA 22092

Robert Reinke
AFWL/NTESG
Kirtland AFB, NM 87117-6008

Dr. Byron Ristvet
HQ DNA, Nevada Operations Office
Attn: NVCG
P.O. Box 98539
Las Vegas, NV 89193

HQ AFTAC/TGR
Attn: Dr. George H. Rothe
Patrick AFB, Florida 32925-6001

Donald L. Springer
Lawrence Livermore National Laboratory
P.O. Box 808, L-205
Livermore, CA 94550

Dr. Lawrence Turnbull
OSWR/NED
Central Intelligence Agency
CIA, Room 5G48
Washington, D.C. 20505

Dr. Thomas Weaver
Los Alamos National Laboratory
P.O. Box 1663
MS C 335
Los Alamos, NM 87545

GL/SULL
Research Library
Hanscom AFB, MA 01731-5000 (2 copies)

Secretary of the Air Force (SAFRD)
Washington, DC 20330
Office of the Secretary Defense
DDR & E
Washington, DC 20330

HQ DNA
ATTN: Technical Library
Washington, DC 20305

DARPA/RMO/RETRIEVAL
1400 Wilson Blvd.
Arlington, VA 22209

DARPA/RMO/Security Office
1400 Wilson Blvd.
Arlington, VA 22209

GL/XO
Hanscom AFB, MA 01731-5000

GL/LW
Hanscom AFB, MA 01731-5000

DARPA/PM
1400 Wilson Boulevard
Arlington, VA 22209

Defense Technical
Information Center
Cameron Station
Alexandria, VA 22314
(5 copies)

Defense Intelligence Agency
Directorate for Scientific &
Technical Intelligence
Washington, D.C. 20301

Defense Nuclear Agency/SPSS
ATTN: Dr. Michael Shore
6801 Telegraph Road
Alexandria, VA 22310

AFTAC/CA (STINFO)
Patrick AFB, FL 32925-6001

Mr. Alfred Lieberman
ACDA/VI-OA'State Department Building
Room 5726
320 - 21St Street, NW
Washington, D.C. 20451

TACTEC
Battelle Memorial Institute
505 King Avenue
Columbus, OH 43201 (Final report only)